Pacific Northwest
NATIONAL LABORATORY

Proudly Operated by **Battelle** *Since 1965*

Spectroscopic Properties of Tc(I) Tricarbonyl Species Relevant to the Hanford Tank Waste

TG Levitskaia
A Andersen
SD Chatterjee
GB Hall
ED Walter
NM Washton

December 2015

DISCLAIMER

This report was prepared as an account of work sponsored by an agency of the United States Government. Neither the United States Government nor any agency thereof, nor Battelle Memorial Institute, nor any of their employees, makes **any warranty, express or implied, or assumes any legal liability or responsibility for the accuracy, completeness, or usefulness of any information, apparatus, product, or process disclosed, or represents that its use would not infringe privately owned rights**. Reference herein to any specific commercial product, process, or service by trade name, trademark, manufacturer, or otherwise does not necessarily constitute or imply its endorsement, recommendation, or favoring by the United States Government or any agency thereof, or Battelle Memorial Institute. The views and opinions of authors expressed herein do not necessarily state or reflect those of the United States Government or any agency thereof.

Spectroscopic Properties of Tc(I) Tricarbonyl Species Relevant to the Hanford Tank Waste

TG Levitskaia
A Andersen
SD Chatterjee
GB Hall
ED Walter
NM Washton

December 2015

Pacific Northwest National Laboratory
Richland, Washington 99352

Summary

Technetium-99 (Tc) exists predominately in soluble forms in the liquid supernatant and salt cake fractions of the nuclear tank waste stored at the U.S. DOE Hanford Site. In the strongly alkaline environments prevalent in the tank waste, its dominant chemical form is pertechnetate (TcO_4^-, oxidation state +7). However, attempts to remove Tc from the Hanford tank waste using ion-exchange processes specific to TcO_4^- only met with limited success, particularly processing tank waste samples containing elevated concentrations of organic complexants. This suggests that a significant fraction of the soluble Tc can be present as non-pertechnetate low-valent Tc (oxidation state < +7) (non-pertechnetate). The chemical identities of these non-pertechnetate species are poorly understood. Previous analysis of the SY-101 and SY-103 tank waste samples provided strong evidence that non-pertechnetate can be comprised of $[Tc(CO)_3]^+$ complexes containing Tc in oxidation state +1 (Lukens et al. 2004). During the last two years, our team has expanded this work and demonstrated that high-ionic-strength solutions typifying tank waste supernatants promote oxidative stability of the $[Tc(CO)_3]^+$ species (Rapko et al. 2013; Levitskaia et al. 2014). It also was observed that high-ionic-strength alkaline matrices stabilize Tc(VI) and potentially Tc(IV) oxidation states, particularly in presence organic chelators, suggesting that the relevant Tc compounds can serve as important redox intermediates facilitating the reduction of Tc(VII) to Tc(I). Designing strategies for effective Tc processing, including separation and immobilization, necessitates understanding the molecular structure of these non-pertechnetate species and their identification in the actual tank waste samples. To-date, only limited information exists regarding the nature and characterization of the Tc(I), Tc(IV), and Tc(VI) species. One objective of this project is to identify the form of non-pertechnetate in the Hanford waste. To do this, we are developing a spectral library of reference non-pertechnetate compounds that can be compared against actual waste samples. The emphasis of the fiscal year 2015 work was Tc(I) tricarbonyl $[Tc(CO)_3]^+$ compounds. The key findings are summarized below.

A series of the reference $[Tc(CO)_3]^+$ compounds was synthesized and characterized by various spectroscopic techniques. It was concluded that aqua coordinated compounds $[Tc(CO)_3(H_2O)_{3-n}(OH)_n]^{1-n}$ are unstable in alkaline solutions and unlikely to be present in the tank wastes. Among tested organic chelators evaluated for the feasibility of the complex formation with $[Tc(CO)_3]^+$ only gluconate and iminodiacetate (IDA) were found to form strong complexes persistent over prolong times, $[Tc(CO)_3 \cdot IDA]^{n-}$ being the most stable. This suggests that $[Tc(CO)_3 \cdot IDA]^{n-}$ and potentially $[Tc(CO)_3 \cdot Gluconate]^{n-}$ is a possible source of non-pertechnetate Tc in Hanford tanks containing elevated levels of organics. As a companion effort, Tc(VI) and Tc(IV) compounds were generated through reduction of TcO_4^-. The reduction products were characterized by EPR spectroscopy and showed stabilization of Tc(VI) species in the liquid phase. In the tank waste, Tc(VI) that can be either present as a stable form, or be generated as an intermediate during the reduction of TcO_4^- to Tc(I). In summary, ***this project developed stable forms of non-pertechnetate Tc including $[Tc(CO)_3 \cdot Ligand]^{n-}$ (where Ligand = IDA or Gluconate) and Tc(VI).*** The stability testing of these non-pertechnetate compounds is discussed in a separate report.

The spectroscopic database of the obtained Tc(I) $[Tc(CO)_3]^+$ compounds and Tc(IV, VI) in 5M $NaNO_3$/variable NaOH or tank waste simulant solution was built using a range of techniques, including ^{99}Tc nuclear magnetic resonance (NMR), infrared (IR) and electron paramagnetic resonance (EPR) spectroscopies. Based on the results of these measurements, ***it is proposed to use NMR, EPR, and IR spectroscopic techniques for Tc speciation analysis in the actual tank waste samples.***

Each individual spectroscopic technique being utilized has its own distinct advantages and will provide fingerprint like information about the individual components of tank waste. IR spectroscopy provides information regarding Tc-CO bonding in the spectral region largely free of interferences and is suitable for analysis of the electronic and geometric structure of Tc compounds containing the $[Tc(CO)_3]^+$ moiety. ^{99}Tc NMR spectroscopy is ideally suited for monitoring diamagnetic Tc(I) and Tc(VII) species. Small changes in ligand substitution result in large changes in chemical shift giving each compound a signature that is readily monitored. EPR spectroscopy is a complimentary technique to ^{99}Tc NMR and provides structural information on paramagnetic Tc species, which are generally of an even numbered oxidation state, and inaccessible via NMR spectroscopy. EPR spectroscopic measurements have very little interference from diamagnetic impurities present in solution, and thus is an ideal technique for studying paramagnetic species in complex mixtures. This work demonstrates that Tc(VI) even at low concentrations generates unique EPR signal suitable for identification of Tc this oxidation state. The observation that Tc(VI) signal persists in the solution simulating tank waste supernatants encourages application of EPR techniques for the analysis of the actual tank wastes.

In conjunction with the aforementioned techniques, density functional theory (DFT) computations are being benchmarked against the empirical results. This allows us to simultaneously pursue two routes towards determination of tank waste composition; characterizing the spectral fingerprints of individual species likely present in tank waste for facile identification of tank waste composition, and developing the capability to computationally predict the chemical structure of spectral signatures not yet catalogued in our database. DFT calculations complement each characterization techniques individually, and this work expanded our understanding of computational parameters. The computations have been validated against our experimental ^{99}Tc NMR and IR results showing excellent agreement between calculated and experimental spectral characteristics, and the work is currently underway to benchmark the calculations against our experimental EPR spectroscopic measurements. Once fully benchmarked the DFT computations will be used to predict species, which are likely present in Hanford tank waste but difficult to synthetically access in a laboratory environment.

Work our team is currently pursuing will expand a comprehensive spectral database for Tc species potentially present in the Hanford tank waste in two directions. The first objective is aimed at the expansion of the available library of non-pertechnetate compounds in different oxidation states and chemical forms. Synthesis and spectroscopic characterization of Tc(I, II) carbonyl nitrosyl and Tc(IV, VI) species is in progress. In companion effort, we are planning to expand the range of characterization techniques. X-ray Absorption Spectroscopy (XAS) can provide concrete evidence on Tc oxidation state as well as its identity of the first coordination sphere, and has been previously utilized to gain information about the nature of non-pertechnetate in actual Hanford tank waste supernatants. We are planning to expand XAS analysis for identification of Tc species in the actual tank waste supernatants of diverse compositions.

Planned testing includes obtaining the actual waste samples collected from various Hanford tanks and their characterization for Tc speciation with NMR, EPR, IR, and XAS spectroscopies.

Acknowledgements

Acronyms and Abbreviations

ATR	attenuated total reflectance
B3LYP	Becke 3-parameter Lee Yang Parr
CC	complexant concentrate
COSMO	COnductor-like Screening MOdel
DFT	density functional theory
DST	double-shell tank
DTPA	diethylenetriamine-N,N,N,N'',N''-pentaacetic acid
EDTA	ethylenediaminetetraacetic acid
EPR	electron paramagnetic resonance
EXAFS	extended X-ray absorption fine structure
FEP	fluorinated ethylene propylene
FTIR	Fourier Transform Infrared
FY	fiscal year
GHz	gigahertz
HEDTA	N-(2-hydroxyethyl)ethylenediamine-N,N',N'-triacetic acid
Hz	Hertz
IDA	iminodiacetic acid
IR	infrared
LAW	low-activity waste
NMR	nuclear magnetic resonance
NTA	nitrilotriacetic acid
PEP	Pretreatment Engineering Platform
PNNL	Pacific Northwest National Laboratory
ppm	parts per million
PTFE	polytetrafluoroethylene
QA	quality assurance
R&D	research and development
RPL	Radiochemical Processing Laboratory
SST	single-shell tank
THF	tetrahydrofuran
TZVPP	triple zeta valence plus polarization
UV	ultraviolet
UV-Vis	ultraviolet-visible
WWFTP	WRPS waste form testing program
XANES	X-ray absorption near edge spectroscopy
XAS	X-ray absorption spectroscopy
ZORA	zero order regular approximation

Contents

Figures

Tables

1.0   Introduction

As described in TP-EMSP-0018[1], Technetuim-99 (^{99}Tc), generated from the fission of ^{235}U and ^{239}Pu, is a major risk-driving component in the liquid fraction of nuclear waste tanks at the DOE Hanford Site in Washington State. Among radioactive constituents in the tank waste, ^{99}Tc presents a unique challenge. The long half-life (β = 292 keV; $T_{1/2}$ = 2.11×10^5 y), complex chemical behavior in tank waste, and high mobility in subsurface environments make Tc one of the most challenging radionuclides to dispose of and/or remediate. Previous attempts to remove Tc from the Hanford tank waste using an ion-exchange process specific to pertechnetate (TcO_4^-) only met with limited success and were particularly less successful for the tank wastes, including tanks SY-101 and SY-103, containing organic complexants such as nitrilotriacetate (NTA), ethylenediaminetetraacetate (EDTA), citrate, and gluconate (Schroeder et al. 1998; Golcar et al. 2000). This suggests that a significant fraction of the soluble Tc can be present as non-pertechnetate low-valent Tc (oxidation state < +7) (non-TcO_4^-). The chemical identities of these non-TcO_4^- species are poorly understood.

X-ray absorption analysis of the waste samples collected from the actual SY-101 and SY-103 tank waste supernatants suggested the presence of the non-pertechnetate species derived from Tc(I) carbonyl moiety (Lukens et al. 2004). During last two years, our PNNL team has expanded this work and demonstrated that high ionic strength solutions typifying tank waste supernatants promote oxidative stability of the *fac*-[Tc(CO)$_3$]$^+$ species[2] (Rapko et al. 2013; Levitskaia et al. 2014). Recent work by our group has significantly expanded this hypothesis, demonstrating that Tc(I) carbonyl compounds can be generated from reduction of TcO_4^- in simulated Hanford tank waste in the presence CO at elevated temperature (Levitskaia et al. 2014), and on-going monitoring of these samples indicates long-term stability of Tc(I) carbonyl and Tc(VI) non-pertechnetate[3]. It also was observed that high ionic strength alkaline matrices stabilize Tc(VI) and potentially Tc(IV) oxidation states, particularly in presence organic chelators, suggesting that the relevant Tc compounds can serve as important redox intermediates facilitating the reduction of Tc(VII) to Tc(I). These results support the hypothesis that Tc(I)-containing [Tc(CO)$_3$]$^+$ species can be a prominent component of Hanford tank waste.

Designing strategies for effective Tc processing, including separation and immobilization, necessitates understanding the molecular structure of these non-pertechnetate species and their identification in the actual tank waste samples. To-date, only limited information exists regarding the nature and characterization of the Tc(I), Tc(IV), and Tc(VI) species. To address this need, the objective of this work is to build a library of the reference non-pertechnetate compounds and their spectroscopic database. The emphasis of the fiscal year 2015 work was [Tc(CO)$_3$]$^+$ compounds.

---

[1] Levitskaia TG and DJ McCabe. 2015. *Technetium Management – Hanford Site (FY 2015)*. TP-EMSP-0018 Rev.1.0, Pacific Northwest National Laboratory, Richland, WA.
[2] All Tc(I) carbonyl compounds described in this report have *facial* octahedral geometry, and in the following text the notation "*fac-*" is omitted for clarity.
[3] These results are outside of the subject of this report and will be summarized in a separate report of Task 3 of the Technetium Management Program.

2.0   Quality Assurance

This work was conducted as part of Pacific Northwest National Laboratory (PNNL) Project 54042 under the Technetium Management Program, with funding from the U.S. Department of Energy Office of Environmental Management.

All research and development (R&D) work at PNNL is performed in accordance with PNNL's laboratory-level Quality Management Program, which is based on a graded application of NQA-1-2000, *Quality Assurance Requirements for Nuclear Facility Applications*, to R&D activities. In addition to the PNNL-wide quality assurance (QA) controls, the QA controls of the WRPS Waste Form Testing Program (WWFTP) QA program were also implemented for the work. The WWFTP QA program consists of the WWFTP Quality Assurance Plan (QA-WWFTP-001) and associated QA-NSLW-numbered procedures that provide detailed instructions for implementing NQA-1 requirements for R&D work. The WWFTP QA program is based on the requirements of NQA-1-2008, *Quality Assurance Requirements for Nuclear Facility Applications*, and NQA-1a-2009, *Addenda to ASME NQA-1-2008 Quality Assurance Requirements for Nuclear Facility Applications*, graded on the approach presented in NQA-1-2008, Part IV, Subpart 4.2, "Guidance on Graded Application of Quality Assurance (QA) for Nuclear-Related Research and Development". Preparation of this report and performance of the associated experimental work were assigned the technology level "Applied Research" and were conducted in accordance with procedure QA-NSLW-1102, *Scientific Investigation for Applied Research*. All staff members contributing to the work have technical expertise in the subject matter and received QA training prior to performing quality-affecting work. The "Applied Research" technology level provides adequate controls to ensure that the activities were performed correctly. Use of both the PNNL-wide and WWFTP QA controls ensured that all client QA expectations were addressed in performing the work.

3.0   Experimental

3.1   Materials

In-house NH_4TcO_4 stock available at the Radiochemical Processing Laboratory (RPL) at PNNL was used. Diglyme, acetonitrile, diethyl ether, dichloromethane, and borane-tetrahydrofuran BH_3/THF complex were obtained from Sigma-Aldrich and used without further purification. Gaseous CO used in the diglyme synthesis of the $(Et_4N)_2[Tc(CO)_3Cl_3]$ was obtained from Matheson Tri-Gas. Argon gas also was obtained from Matheson. All inorganic sodium salts (including carbonate, oxalate, gluconate, nitrilotriacetate (NTA), iminodiacetate (IDA) nitrate, nitrite, hydroxide, and sulfate) and aluminum nitrate were obtained from Sigma-Aldrich and were of reagent grade. All aqueous solutions were prepared from distilled water deionized to ≥ 15 MΩ cm with a Barnstead Nanopure water purification system.

Caustic solution simulating Hanford tank waste supernatants was prepared following a procedure previously developed for the Pretreatment Engineering Platform (PEP) testing (Scheele et al. 2009), albeit with a reduced NaOH concentration. The composition of the simulant is given in Table 1.

Table 1. PEP Supernatant Simulant Composition (Levitskaia et al. 2014)

Constituent	Target Concentration	
	μg/mL	M
Al^{3+}	5,900	0.217
Na^+	108,700	4.73
$C_2O_4^{2-}$	<450	<0.005
NO_2^-	25,300	0.55
NO_3^-	104,800	1.69
PO_4^{3-}	15,100	0.158
SO_4^{2-}	19,200	0.200
CO_3^{2-}	7,360	0.613
OH^-	18,800	0.47

3.2 Synthesis of $[Tc(CO)_3]^+$ Compounds

Solid $(Et_4N)_2[Tc(CO)_3Cl_3]$ compound was prepared by a two-step reduction procedure. First Tc(VII) in ammonium pertechnetate was reduced to Tc(V) and isolated as $(Bu_4N)[TcOCl_4]$ solid, which was subsequently reduced in the presence of CO to Tc(I) in the chemical form of $[Tc(CO)_3Cl_3]^{2-}$ as described elsewhere (Levitskaia et al. 2014). The $(Et_4N)_2[Tc(CO)_3Cl_3]$ product was separated by precipitation. In a companion effort the second reduction step was repeated using ^{13}C-labelled CO to obtain $(Et_4N)_2[Tc(^{13}CO)_3Cl_3]$. The NMR-active ^{13}C isotope provides for additional compound characterization means and confirmation of the Tc(I) product structure as well as better understanding of the coordination environment around the Tc center.

The $(Et_4N)_2[Tc(CO)_3Cl_3]$ compound was used to generate analytically pure tetrameric $[Tc(CO)_3(OH)]_4$ species according to the modified literature procedure (Alberto et al. 1998) by dissolution in NaOH solution, extraction into diethyl ether, and crystallization from dichloromethane. The ^{13}C-labelled analog was prepared using $(Et_4N)_2[Tc(^{13}CO)_3Cl_3]$ material.

$(Et_4N)_2[Tc(CO)_3Cl_3]$ and $[Tc(CO)_3(OH)]_4$ products were used to generate other Tc(I) tricarbonyl complexes for the subsequent studies.

The $[Tc(CO)_3]^+$ aqua species of the general formula $[Tc(CO)_3(H_2O)_{3-n}(OH)_n]^{1-n}$ (n = 0 – 3) were obtained by dissolving $(Et_4N)_2[Tc(CO)_3Cl_3]$ or $[Tc(CO)_3(OH)]_4$ precursor in 5 M $NaNO_3$ containing variable NaOH concentrations or simulant solution.

To build a spectroscopic library of the $[Tc(CO)_3]^+$ complexes with small chelators found in the Hanford tanks, these compounds were prepared using similar a procedure previously employed to obtain $[Tc(CO)_3]^+$•Gluconate complex (Levitskaia et al. 2014). In a general synthetic procedure, $(Et_4N)_2[Tc(CO)_3Cl_3]$ or $[Tc(CO)_3(OH)]_4$ was allowed to react with a solution of 0.1 M chelator solution in 5 M $NaNO_3$/0.1 M NaOH or simulant. The tested chelators include formate, acetate, citrate, glycolate, gluconate, iminodiacetic acid (IDA), nitrilotriacetic acid (NTA), ethylenediaminetetraacetic acid (EDTA), N-(2-hydroxyethyl)ethylenediamine-N,N',N'-triacetic acid (HEDTA), and diethylenetriamine-N,N,N,N'',N''-pentaacetic acid (DTPA). The molecular structures of these compounds are shown in Figure 1.

The protocol for the complexation reaction using $(Et_4N)_2[Tc(CO)_3Cl_3]$ starting material is as follows:

- Prepare $4 - 5$ mM $(Et_4N)_2[Tc(CO)_3Cl_3]$ solution in 5 M $NaNO_3$/0.1 M NaOH or in simulant;
- Prepare 0.1 M chelator solution in 5 M $NaNO_3$/0.1 M NaOH or in simulant;
- Add 1 mL of Tc solution to 1 mL of the chelator solution. Monitor complex formation by ^{99}Tc NMR spectroscopy. In aqueous alkaline solution, the chloride ligands of the $[Tc(CO)_3Cl_3]^{2-}$ complex are exchanged by water and hydroxide, forming $[Tc(CO)_3(H_2O)_2(OH)]$ species, which show a single Tc resonance at -1068 ppm. The complexation behavior was monitored via the reduction of the -1068 ppm and appearance of the new resonance due to complex formation.
- If the $[Tc(CO)_3]^+$•Ligand complex was not formed, increase chelator concentration and continue monitoring by ^{99}Tc NMR.

It appeared that when the same protocol as described above was utilized for $[Tc(CO)_3(OH)]_4$ starting material, the kinetics of complex formation was impractically slow, indicating high stability of the $[Tc(CO)_3(OH)]_4$ tetramer towards formation of the monomeric $[Tc(CO)_3(H_2O)_2(OH)]$ analog and ligand substitution. Therefore, $[Tc(CO)_3(OH)]_4$ was first converted to the $[Tc(CO)_3(H_2O)_3]^+$ species by dissolution in 1 M triflic acid, extraction into diethyl ether, and crystallization. Solid $[Tc(CO)_3(H_2O)_3]^+$ material was dissolved in 5 M $NaNO_3$/0.1 M NaOH or in simulant, mixed with the chelator solution, and monitored by ^{99}Tc NMR as described above.

3.3 Electrochemical Synthesis of Tc(IV) and Tc(VI) Compounds

Controlled potential electrolysis methods were used for the electrochemical reduction of TcO_4^- using a standard three-electrode cell stand and a Epsilon Potentiostat from Bioanalytical Systems (BASi), Indiana, USA.

Reduction was conducted in a BASi thin layer absorbance cell (1 mm path length). For cyclic voltammetry and controlled potential electrolysis measurements, a platinum mesh was used as a working electrode. All reported potentials were referenced versus a Ag/AgCl micro-electrode and a platinum wire was used at the auxiliary electrode. For the reduction of TcO_4^- to Tc(VI), a platinum 100 mesh electrode from Sigma-Aldrich (99.9%) was used as the working electrode. For the reduction to Tc(IV), a platinum coil electrode was used as the working electrode, onto which the Tc(IV) was electrodeposited by application of the appropriate reduction potential.

Reduction of Tc(VII) to Tc(VI) was confirmed by spectroelectrochemical technique employing absorption-based double potential step chronoabsorptometry. In a typical experiment, the initial potential was set to -0.1 V to ensure that the entire Tc concentration in the sample was in the fully oxidized TcO_4^- state, while absorption spectra were concurrently recorded. Subsequently, the working potential was set to a given value (E_{app}) and the solution was allowed to reach equilibrium, which was inferred when the UV-visible absorption spectrum no longer changed over a 3–4 min period. For spectroelectrochemistry measurements, a platinum 100 mesh electrode from Sigma-Aldrich (99.9%) was used as the working electrode. UV absorption spectra were recorded with a deuterium light source (Mikropack, model# DH 2000) and an Ocean Optics USB2000 detector (188-880 nm) using Spectra Suite Software for spectral data acquisitions. Spectroelectrochemical titration data thus obtained were analyzed according to the Nernstian expression (1) for a multi-electron transfer reaction:

$$E_{app} = E^{0\prime} - \frac{0.0591}{n} \log \frac{[Red]}{[Ox]} \tag{1}$$

where $E^{0\prime}$ is the formal electrode potential, n is the number of electrons transferred, and [Red] and [Ox] are the respective concentrations of the fully reduced and fully oxidized species. The ratio [Red]/[Ox] at applied potential E_{app} was estimated from $(A_{ox}-A)/(A-A_{red})$, where A is the absorbance at a given wavelength. A_{ox} is the absorbance of the fully oxidized species, which was estimated from the absorbance at the most positive value of E_{app} (E_{app} = -0.1 V; where [Ox]/[Red] > 1000); A_{red} is the absorbance of the fully reduced sample, which was estimated from the absorbance at the most negative value of E_{app} (E_{app} = -0.8 V; where [Ox]/[Red] < 0.001) (Schroll et al. 2012).

DTPA

HEDTA

EDTA

Glycolic acid

Iminodiacetic acid

Nitrilotriacetic acid

Citric acid

Sodium gluconate

Sodium formate

Sodium acetate
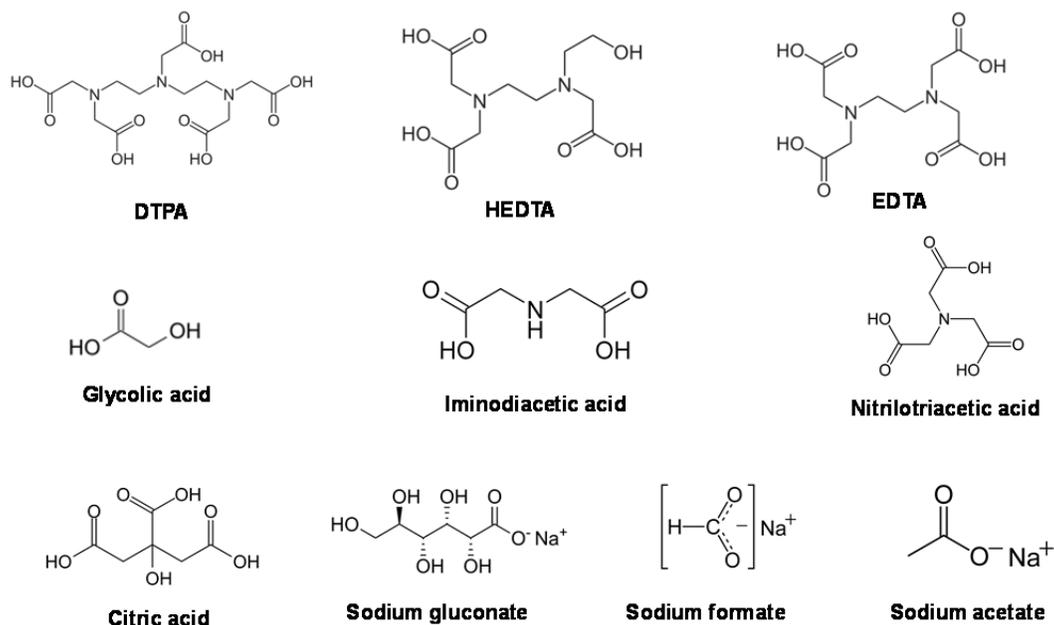
Figure 1. Molecular Structure of the Small Organic Chelators Tested for Complex Formation with $[Tc(CO)_3]^+$

3.4   Spectroscopic Characterization

A range of spectroscopic techniques were utilized to characterize different $[Tc(CO)_3]^+$ species and build the spectroscopic library that can be used to effectively identify the different $[Tc(CO)_3]^+$ species as well as distinguish them from each other and from the other Tc species potentially present in the LAW fraction of the Hanford tank waste.

Technetium-99 nuclear magnetic resonance (NMR) spectroscopy. The NMR sample solutions were placed in capped polytetrafluoroethylene (PTFE)/fluorinated ethylene propylene (FEP) copolymer sleeves (Wilmad Lab Glass, Vineland, NJ), which were then inserted into 5- or 10-mm glass NMR tubes to provide secondary containment for the radioactive liquid. Technetium-99 NMR data were routinely collected at 67.565 MHz on a Tecmag Discovery spectrometer equipped with a 10-mm broadband Nalorac probe as described previously (Cho et al. 2004). A solution containing 10 mM TcO_4^- was used as a Tc-99 chemical shift reference, and all chemical shift data are quoted relative to TcO_4^- (Franklin et al. 1982).

Fourier Transform Infrared (FTIR) spectroscopy. FTIR measurements were conducted using a spectrometer (ALPHA model, Bruker Optics) operated with OPUS software (Version 6.5 Build 6.5.92). Samples were run directly on a diamond attenuated total reflectance (ATR) cell. For each sample, 24 scans with a resolution of 4 wavenumbers (cm^{-1}) were averaged to give the final spectrum. A background of ambient air was used for all samples. A sample volume of approximately 10 μL was used for each analysis; this was adequate to cover the collection region of the ATR cell.

Technetium-99 electron paramagnetic resonance (EPR) spectroscopy. EPR spectra were acquired on a Bruker EMX Spectrometer equipped with an ER4102ST resonator (spectra at room temperature and 120 K) or an ER4116DM Dual Mode resonator (spectra at 5 K) and an Oxford ESR910 cryostat. Samples were doubly contained by employing unbreakable FEP tube liners (Wilmad Lab Glass, Vineland, NJ) inside traditional quartz EPR tubes. Liquid samples employed 1.5 -mm inner diameter (ID) liners and 4 mm outer diameter (OD) quartz tubes while frozen solution and powder samples used 3.15 mm ID liners and 5 mm OD tubes.

3.5 Theoretical Calculations

Density Functional Theory (DFT) computations were carried out using the ORCA software program (Neese 2012) utilizing the B3LYP functional, def2-TZVPP basis set (Schäfer et al. 1992; Weigend and Ahlrichs 2005). Solvation effects where accounted for using COSMO with appropriate dielectric constant and polarizability for each solvent examined. Relativistic effects were handled using the zeroth order regular approximation (ZORA) to the Dirac equation. Computations were performed on clusters available through PNNL Institutional Computing (PIC).

4.0   Results

4.1 Characterization of $[Tc(CO)_3]^+$ by Solution ^{99}Tc NMR Spectroscopy

NMR spectroscopy looks at the transition of a nuclear spin in a magnetic field from a low energy state in line with the magnetic field to a high energy state opposing the magnetic field. When placed in a magnetic field, NMR-active nuclei (such as ^{1}H, ^{13}C, or ^{99}Tc) absorb electromagnetic radiation at a frequency characteristic of the isotope. The excited nuclei subsequently emit this radiation in the form of a nuclear free induction decay, which is characteristic not only to the type of nucleus but also to the electronic environment of the nucleus determined by the molecular structure. Upon application of the external magnetic field, the electrons in the vicinity of a nucleus create a local magnetic field that "shields" the nuclei from the external magnetic field, affecting the required excitation energy. Different electronic environments of the nuclei result in different amount of shielding and generate unique NMR spectra characteristic for the corresponding chemical structures. For the NMR-active ^{99}Tc nucleus, the odd oxidation states of +1 and +7 with low spin are particularly suitable for NMR spectroscopy. It is noteworthy that Tc in the oxidation state + 7 and corresponding chemical form of pertechnetate TcO_4^- has been observed by NMR in Hanford tank wastes (Rapko et al. 2003). Literature and our studies of $[Tc(CO)_3]^+$ compounds have indicated that they generate distinct NMR spectra exhibiting significant differences in their chemical shifts and line widths determined by the nature of the auxiliary ligands at detection limit and sensitivity very similar to those of pertechnetate (Gorshkov et al. 2000; Levitskaia et

al. 2014) and therefore can be potentially determined in the tank waste supernatants by ^{99}Tc NMR spectroscopy.

4.1.1   [99]Tc NMR Spectroscopy of the Starting Materials

4.1.1.1   (Et$_4$N)$_2$[Tc(CO)$_3$Cl$_3$]

Building a reliable spectral database suitable for the identification of the [Tc(CO)$_3$]$^+$ compounds in tank waste requires careful characterization and verification of the purity of the starting (Et$_4$N)$_2$[Tc(CO)$_3$Cl$_3$] and [Tc(CO)$_3$(OH)]$_4$ materials used to generate other [Tc(CO)$_3$]$^+$ derivatives. Oxidation state purity of Tc(I) and chemical structure of the synthesized (Et$_4$N)$_2$[Tc(CO)$_3$Cl$_3$] and [Tc(CO)$_3$(OH)]$_4$ products were confirmed by NMR spectroscopy described in this section and other techniques described in this report. It should be noted that the (Et$_4$N)$_2$[Tc(CO)$_3$Cl$_3$] compound is not expected to be present in the tank waste because it readily exchanges weakly coordinating Cl$^-$ ligands with water, hydroxide, and small organic chelators found in the tank waste. On the other hand, [Tc(CO)$_3$(OH)]$_4$ tetramer species can potentially be present in the brine-like tank supernatants in which the activity of free water is low enough to effectively solvate these species and facilitate their dissociation to the monomeric species.

Since (Et$_4$N)$_2$[Tc(CO)$_3$Cl$_3$] readily exchanges Cl$^-$ ligands with water and is not present in the aqueous solutions at concentration levels sufficient for NMR analysis, it was characterized in organic solvents. The ^{99}Tc NMR spectrum of (Et$_4$N)$_2$[Tc(CO)$_3$Cl$_3$] in acetonitrile shows two sharp resonances at -1128 and -1136 ppm (Figure 2), suggesting two different [Tc(CO)$_3$]$^+$ chemical environments for Tc. Alberto and coworkers have shown that in the presence of MeCN, facile exchange of chloride in the [Tc(CO)$_3$Cl$_3$]$^{2-}$ complex can occur to form [Tc(CO)$_3$(MeCN)$_3$]$^+$ (Alberto et al. 1995). The ^{99}Tc NMR resonance of the [Tc(CO)$_3$(MeCN)$_3$]$^+$ complex was reported at -2853 ppm (Mikhalev 2005). Based on this information, the observed -1128 and -1136 ppm resonances were tentatively assigned to the mixed [Tc(CO)$_3$Cl$_n$(MeCN)$_{3-n}$]$^{1-n}$ complex species. On the other hand, the ^{99}Tc NMR spectrum of (Et$_4$N)$_2$[Tc(CO)$_3$Cl$_3$] in THF showed a single resonance at -970 ppm (Figure 2) consistent with the [Tc(CO)$_3$Cl$_3$]$^{2-}$ species. No resonances due to other Tc(I) species or Tc(VII), TcO$_4^-$, were observed in both spectra collected in MeCN and THF. NMR spectra acquired in a different spectral window around +4000 ppm demonstrated the absence of Tc(V) species in the sample solutions (spectra not shown). These results confirm the Tc(I) oxidation state purity of the (Et$_4$N)$_2$[Tc(CO)$_3$Cl$_3$] compound. It is worth mentioning that that the generated species exhibit a high stability in both MeCN and THF solvents, revealing an identical spectrum for prolonged time (over a month), with no oxidative decomposition TcO$_4^-$.
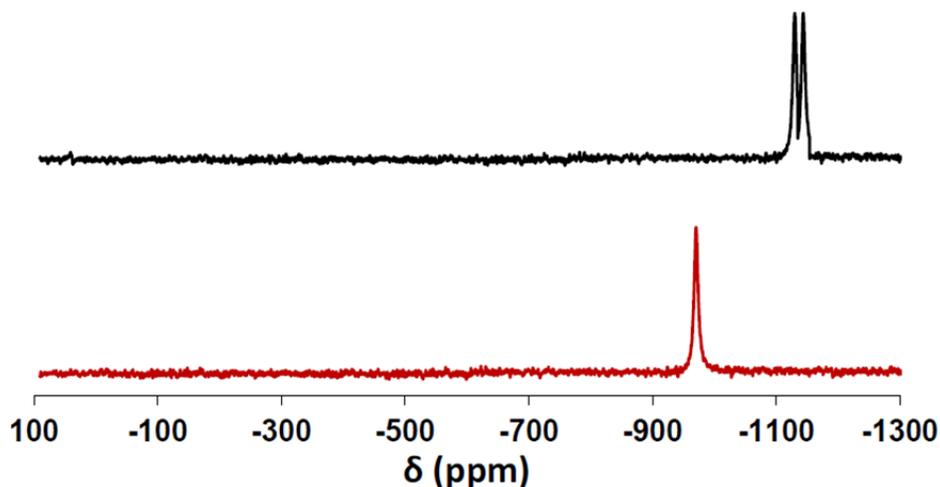
Figure 2. ^{99}Tc NMR Spectra of the $(Et_4N)_2[Tc(CO)_3Cl_3]$ Solution in MeCN (upper, black trace) and THF (bottom, red trace). Spectrum in MeCN shows two resonances at -1128 and -1136 ppm assigned to $[Tc(CO)_3Cl_n(MeCN)_{3-n}]^{1-n}$ species. Spectrum in THF shows one resonance at -970 ppm assigned to $[Tc(CO)_3Cl_3]^{2-}$.

The ^{99}Tc NMR spectrum of the complex $(Et_4N)_2[Tc(^{13}CO)_3Cl_3]$ obtained during the reaction of $[TcOCl_4^-]$ with labeled ^{13}CO shows a similar resonance at -973 ppm (Figure 3) in THF solvent, which is split into a quartet due to $^1J_{99Tc,13C}$ coupling of the ^{99}Tc nucleus bonded with three NMR active ^{13}C nuclei. The $^1J_{99Tc,13C}$ coupling constant is determined to be 354 Hz. To our knowledge, it is the first experimental ^{99}Tc-^{13}C coupling constant reported in organic solvent. The small change in chemical shift of ~3 ppm observed using non-labeled and labeled CO is consistent with the substitution of ^{12}CO for ^{13}CO ligands (Aebischer et al. 2000). This characteristic splitting of the Tc(I) resonance unambiguously confirms the presence of the $[Tc(CO)_3]^+$ core in the molecular structure.
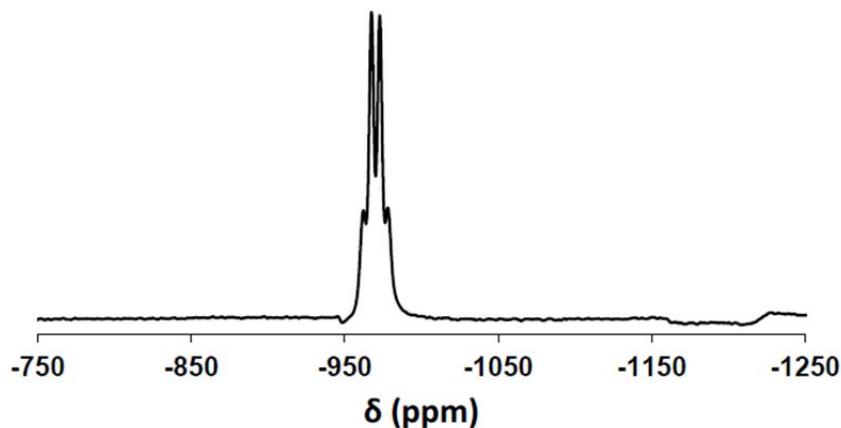
Figure 3. ^{99}Tc NMR Spectrum of the $(Et_4N)_2[Tc(^{13}CO)_3Cl_3]$ Solution in THF

4.1.1.2 [Tc(CO)₃(OH)]₄

The ^{99}Tc NMR spectra of [Tc(CO)$_3$(OH)]$_4$ acquired in aqueous and organic solvents show a single Tc(I) resonance (Figure 4) suggesting presence of a single [Tc(CO)$_3$]$^+$ species. No other Tc resonances due to Tc(VII) or Tc(V) were observed by NMR spectroscopy, confirming Tc(I) oxidation state purity. In aqueous 5 M NaNO$_3$ solution, a Tc(I) resonance appears at -583 ppm, corroborating the [Tc(CO)$_3$(OH)]$_4$ structure (Gorshkov et al. 2000; Levitskaia et al. 2014). This resonance shifts downfield in organic solvents due to less-effective solvation and appears at -548 ppm in diethyl ether and at -490 ppm in acetonitrile and dichloromethane.
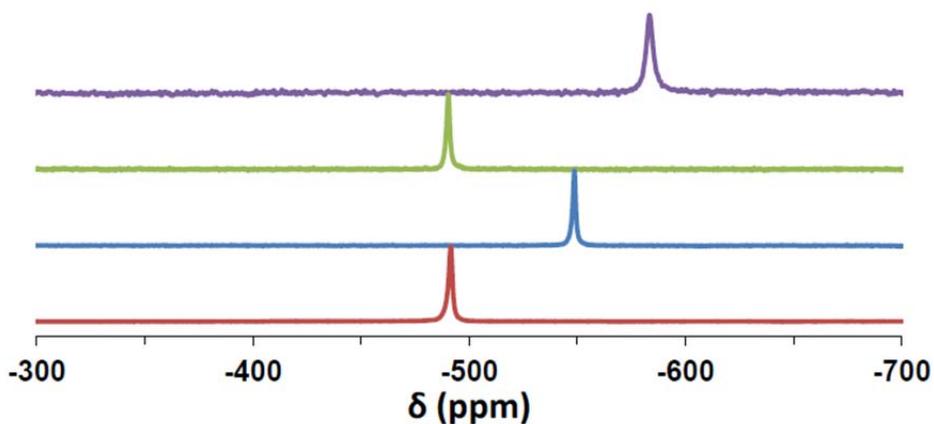
Figure 4. Solution ^{99}Tc NMR Spectra of [Tc(CO)$_3$(OH)]$_4$ in Aqueous 5 M NaNO$_3$ (upper, violet trace), MeCN (second from the top, green trace), Et$_2$O (second from the bottom, blue trace), and Dichloromethane (bottom, red trace)

The ^{99}Tc NMR spectrum of the labeled [Tc(^{13}CO)$_3$(OH)]$_4$ material obtained using [Tc(^{13}CO)$_3$Cl$_3$]$^{2-}$ precursor shows a quartet resonance at -586 ppm in the aqueous 5 M NaNO$_3$ solution (Figure 5). As for [Tc(^{13}CO)$_3$Cl$_3$]$^{2-}$, the quartet splitting is due to $^1J_{99Tc,13C}$ coupling of the ^{99}Tc nucleus with three NMR-active ^{13}C nuclei bonded to it. The $^1J_{99Tc,13C}$ coupling constant is 385 Hz.
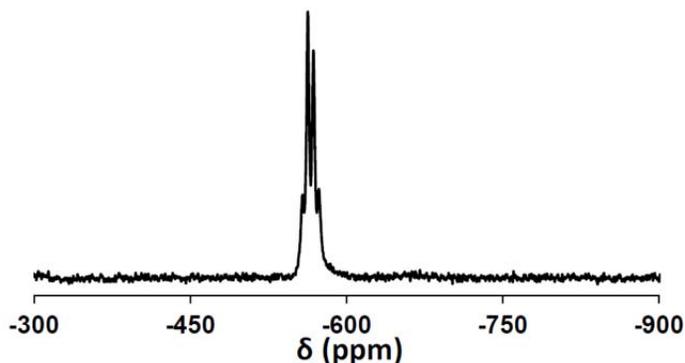
Figure 5. ^{99}Tc NMR Spectrum of [Tc(^{13}CO)$_3$(OH)]$_4$ in Aqueous 5 M NaNO$_3$ Solution

4.1.2 Solution ^{99}Tc NMR Spectroscopy of $[Tc(CO)_3(H_2O)_{3-n}(OH)_n]^{1-n}$

In our previous work, we have gained an understanding of the hydrolysis behavior and chemical speciation of the $[Tc(CO)_3]^+$ species in aqueous high-salt alkaline solutions in the absence of small organic chelators (Rapko et al. 2013; Levitskaia et al. 2014). These species are represented by the general formula $[Tc(CO)_3(H_2O)_{3-n}(OH)_n]^{1-n}$ (n = 0 – 3) and include $[Tc(CO)_3(H_2O)_3]^+$, $[Tc(CO)_3(H_2O)_2(OH)]$, $[Tc(CO)_3(H_2O)(OH)_2]^-$, and $[Tc(CO)_3(OH)_3]^{2-}$. The formation of these individual species depends upon the solution pH and OH$^-$ concentrations. Additionally, the tetrameric species $[Tc(CO)_3(OH)]_4$ can form at high $[Tc(CO)_3]^+$ concentration, within the pH range of 7 – 11. An objective of this work was to build a spectroscopic library of these complexes. The $[Tc(CO)_3(H_2O)_{3-n}(OH)_n]^{1-n}$ products were obtained by dissolving $(Et_4N)_2[Tc(CO)_3Cl_3]$ or $[Tc(CO)_3(OH)]_4$ precursor in 5 M NaNO$_3$ containing variable NaOH concentrations or simulant solution.

4.1.2.1 5 M NaNO$_3$/Variable NaOH Solutions

The ^{99}Tc NMR spectra of the $[Tc(CO)_3(H_2O)_{3-n}(OH)_n]^{1-n}$ products obtained by dissolution of the $[Tc(CO)_3Cl_3]^{2-}$ precursor in the 5 M NaNO$_3$ solution at variable pH are shown in Figure 6. The detailed speciation analysis and corresponding NMR assignment are reported elsewhere (Gorshkov et al. 2000; Rapko et al. 2013; Levitskaia et al. 2014), and only a brief summary is given in this report.

Tc(I) tricarbonyl triaqua $[Tc(CO)_3(H_2O)_3]^+$ species existing in the acidic solutions exhibit a single narrow (line width ~ 80 Hz) resonance at -868 ppm. The NMR spectrum remains largely invariant within the pH range between 0 and about 6, suggesting that $[Tc(CO)_3(H_2O)_3]^+$ is the predominant $[Tc(CO)_3]^+$ component at acidic to near-neutral pH. In near-neutral and mildly alkaline solutions with pH between 6.5 and about 11, the first hydrolysis products, including monomeric mono-hydroxo $[Tc(CO)_3(H_2O)_2(OH)]$ and/or tetrameric analog $[Tc(CO)_3(OH)]_4$ species, are formed as evident from the corresponding Tc NMR resonances appearing at -1070 and -585 ppm, respectively. For solutions with a pH > 11 and a hydroxide concentration up to approximately 1 M, $[Tc(CO)_3(H_2O)_2(OH)]$ is the predominant $[Tc(CO)_3]^+$ component. Further increase of the hydroxide concentration to about 3 M results in appearance of an additional resonance at about -1140 ppm, which is assigned to the second hydrolysis product $[Tc(CO)_3(H_2O)(OH)_2]^-$. It was observed that $[Tc(CO)_3(H_2O)_2(OH)]$ and $[Tc(CO)_3(H_2O)(OH)_2]^-$ species exist at equilibrium up to about 10 M hydroxide concentration. At 10 M NaOH and above, both species disappear and a third hydrolysis product, $[Tc(CO)_3(OH)_3]^{2-}$, is formed as evident from the appearance of a new resonance at -1215 ppm. While these species have not been experimentally observed before, this assignment is consistent with the progressive downfield shift of the ^{99}Tc NMR resonances corresponding to the $[Tc(CO)_3(H_2O)_{3-n}(OH)_n]^{1-n}$ products as the number of electron-rich hydroxide ligands in the complex structure increases. It is to be noted that at the high hydroxide concentrations, a significant amount of TcO$_4^-$ is generated along with the $[Tc(CO)_3(H_2O)_{3-n}(OH)_n]^{1-n}$ species. However, in the presence of high (5 M) NaNO$_3$ concentration, the rate of Tc(I) oxidation is significantly lower than in less concentrated solutions.

Dissolution of the $[Tc(CO)_3(OH)]_4$ complex in 5 M NaNO$_3$ at various pH generated identical $[Tc(CO)_3(H_2O)_{3-n}(OH)_n]^{1-n}$ species and corresponding NMR spectra as using $[Tc(CO)_3Cl_3]^{2-}$ precursor (Figure 7). The slightly different progression of the $[Tc(CO)_3]^+$ hydrolysis as a function of pH was attributed to the slow kinetics of the fragmentation of the $[Tc(CO)_3(OH)]_4$ tetramer which persisted in the wider pH range for the prolonged time. This, however, will not affect identification of the $[Tc(CO)_3(H_2O)_{3-n}(OH)_n]^{1-n}$ species in the actual tank waste samples.
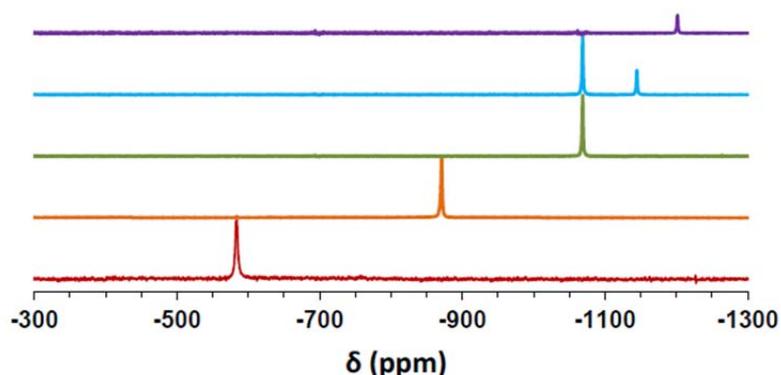
Figure 6. Solution ^{99}Tc NMR Spectra of the $[Tc(CO)_3(H_2O)_{3-n}(OH)_n]^{1-n}$ Species Obtained from $[Tc(CO)_3Cl_3]^{2-}$ in 5 M NaNO$_3$ at Variable pH. Bottom, red trace: $[Tc(CO)_3(OH)]_4$ at pH = 6.5 – 11 (δ = -585 ppm). Second from the bottom, orange trace: $[Tc(CO)_3(H_2O)_3]^+$ at pH = 0 – 6 (δ = -868 ppm). Middle, green trace: $[Tc(CO)_3(H_2O)_2(OH)]$ at [OH$^-$] = 0.1 – 3 M (δ = -1070 ppm). Second from the top, light blue trace: $[Tc(CO)_3(H_2O)_2(OH)]$ and $[Tc(CO)_3(H_2O)(OH)_2]^-$ at [OH$^-$] = 6 M (δ = -1070 and -1140 ppm). Top, violet trace: $[Tc(CO)_3(OH)_3]^{2-}$ at [OH$^-$] = 10 M (δ = -1215 ppm).
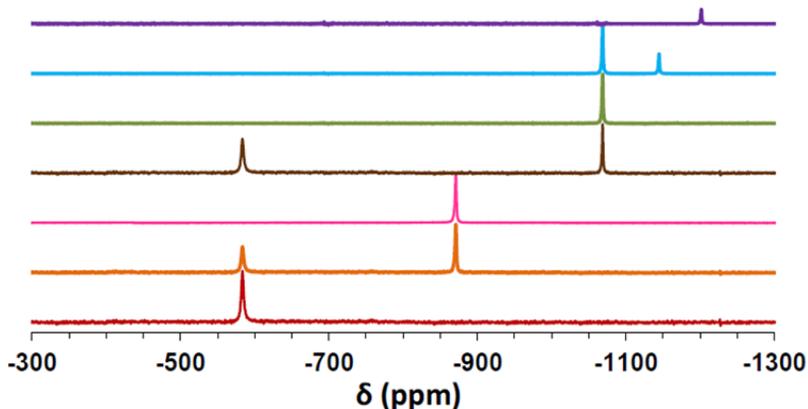
Figure 7. Solution ^{99}Tc NMR Spectra of the $[Tc(CO)_3(H_2O)_{3-n}(OH)_n]^{1-n}$ Species Obtained from $[Tc(CO)_3(OH)]_4^-$ in 5 M NaNO$_3$ at Variable pH. Bottom, red trace: $[Tc(CO)_3(OH)]_4$ at pH = 6.5 – 11 (δ = -585 ppm). Second from the bottom, orange trace: $[Tc(CO)_3(OH)]_4$ and $[Tc(CO)_3(H_2O)_3]^+$ at pH = 2 – 6 (δ = -585 and -868 ppm, respectively). Third from the bottom, pink trace: $[Tc(CO)_3(H_2O)_3]^+$ at pH = 0 – 2 (δ = -868 ppm). Middle, brown trace: $[Tc(CO)_3(OH)]_4$ and $[Tc(CO)_3(H_2O)_2(OH)]$ at pH = 12 (δ = -585 and -1070 ppm, respectively). Third from the top, green trace: $[Tc(CO)_3(H_2O)_2(OH)]$ at [OH$^-$] = 1 – 3M (δ = -1070 ppm). Second from the top, light blue trace: $[Tc(CO)_3(H_2O)_2(OH)]$ and $[Tc(CO)_3(H_2O)(OH)_2]^-$ at [OH$^-$] = 6 M (δ = -1070 and -1140 ppm). Top, violet trace: $[Tc(CO)_3(OH)_3]^{2-}$ at [OH$^-$] = 10 M (δ = -1215 ppm).

4.1.2.2   Simulant Solutions

The dissolution of the $(Et_4N)_2[Tc(CO)_3Cl_3]$ and $[Tc(CO)_3(OH)]_4$ precursors in the simulant resulted in the formation of $[Tc(CO)_3(H_2O)_2(OH)]$ as evident from the Tc(I) NMR resonance at -1068 ppm (Figure 8). The conversion of $[Tc(CO)_3(OH)]_4$ tetramer to the monomeric species was not complete due to the slow fragmentation kinetics. The NMR spectrum (resonance at -585 ppm) shows that a significant $[Tc(CO)_3]^+$ fraction remains in the tetrameric form. In addition, partial oxidation of $[Tc(CO)_3]^+$ to TcO_4^- was observed.
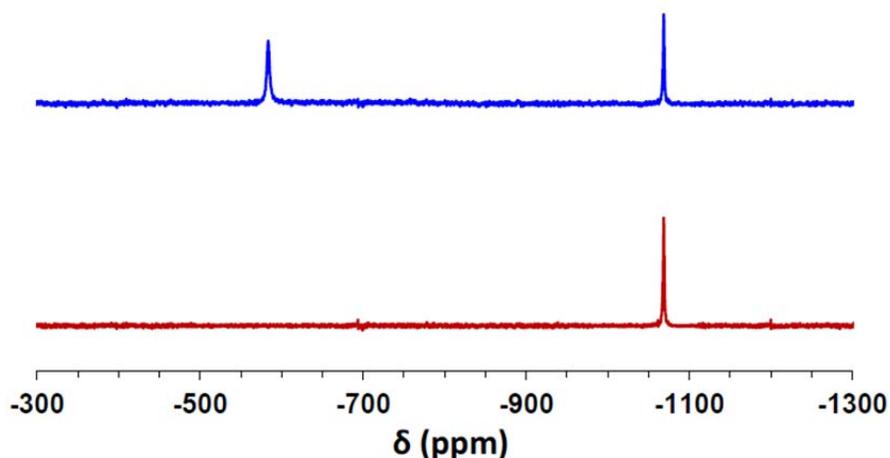
Figure 8.   Simulant Solution ^{99}Tc NMR Spectra of $[Tc(CO)_3(H_2O)_2(OH)]$ (δ = -1070 ppm) Obtained by Dissolution of $[Tc(CO)_3Cl_3]^{2-}$ (bottom, red trace) and $[Tc(CO)_3(OH)]_4$ (top, blue trace)

4.1.3   Solution ^{99}Tc NMR Spectroscopy of $[Tc(CO)_3 \bullet Ligand]^{n-}$ Complexes

In the previous work, we have observed formation of the $[Tc(CO)_3 \bullet Gluconate]^{n-}$ complex in the alkaline solutions simulating Hanford tank waste supernatants and characterized its spectroscopic properties (Levitskaia et al. 2014). This work has been expended to evaluate feasibility of the complex formation of $[Tc(CO)_3]^+$ species with other small chelators found in the Hanford tanks, including formate, acetate, citrate, glycolate, gluconate, iminodiacetic acid (IDA), nitrilotriacetic acid (NTA), ethylenediaminetetraacetic acid (EDTA), N-(2-hydroxyethyl)ethylenediamine-N,N',N'-triacetic acid (HEDTA), and diethylenetriamine-N,N,N,N'',N''-pentaacetic acid (DTPA). The complex formation of $[Tc(CO)_3]^+$ with different chelators in 5 M $NaNO_3$/0.1 M NaOH and simulant solutions was monitored by ^{99}Tc NMR spectroscopy. Identical results were observed when either $(Et_4N)_2[Tc(CO)_3Cl_3]$ or $[Tc(CO)_3(H_2O)_3]^+$ (generated from $[Tc(CO)_3(OH)]_4$ as described in Section 3.0) precursors were used in the complexation reaction. Upon dissolution in 5 M $NaNO_3$/0.1 M NaOH and simulant solutions, both precursors generated the hydrolysis product $[Tc(CO)_3(H_2O)_2(OH)]$, which is reacted with the chelator present in the solution. The complexation results and the observed NMR characteristics of the complex compounds are summarized in Table 2.

Table 2. Complexation Results and the Observed NMR Characteristics of the $[Tc(CO)_3 \cdot Ligand]^{n-}$ Complex Compounds Obtained Using $(Et_4N)_2[Tc(CO)_3Cl_3]$ or $[Tc(CO)_3(H_2O)_3]^+$ Precursors in 5 M $NaNO_3$/0.1 M NaOH or Simulant

Chelator	Complexation	^{99}Tc NMR Chemical shift (ppm)	Half Width of ^{99}Tc Resonance, Hz
DTPA	Yes	-915	600
EDTA	Yes	-916	550
IDA	Yes	-850 (broad)	1000
		-998	700
NTA	Yes	-918	550
Gluconate	Yes	-1100 (broad)	1000
		-1232	650
		-1254	550
Citrate	No	n/a	n/a
Formate	No	n/a	n/a
Acetate	No	n/a	n/a
Glycolate	No	n/a	n/a

No complexation of $[Tc(CO)_3]^+$ with formate, acetate, citrate, glycolate, or HEDTA was observed, as reflected by the absence of the changes in NMR spectra of the starting $[Tc(CO)_3(H_2O)_2(OH)]$ complex in the presence of the ligand. Three polyaminocarboxylate ligands, including EDTA, NTA, and DTPA, exhibited weak coordination, so that only a small fraction of $[Tc(CO)_3]^+$ converted to the complex $[Tc(CO)_3 \cdot Ligand]^{n-}$ compounds, while a significant fraction of $[Tc(CO)_3]^+$ remained as $[Tc(CO)_3(H_2O)_2(OH)]$. The complexation was significantly weaker in the simulant solution, presumably due to the competition with free hydroxide present in the simulant at a 0.5 M concentration. The corresponding NMR spectra are show in Figure 9, Figure 10, and Figure 11. It should be noted that additional small resonances appeared at about -1224 ppm in the presence of EDTA, NTA, and DTPA chelators, suggesting that Tc(I) is present in two different chemical environments. It is interesting that NMR spectra observed for the $[Tc(CO)_3 \cdot Ligand]^{n-}$ complexes, where Ligand = EDTA, NTA, or DTPA, are very similar, indicating nearly identical first coordination shell of the Tc(I) species. This finding is surprising considering that these chelators possess different number of donor groups (even though they are similar in chemical and electronic nature) and different steric constrains.
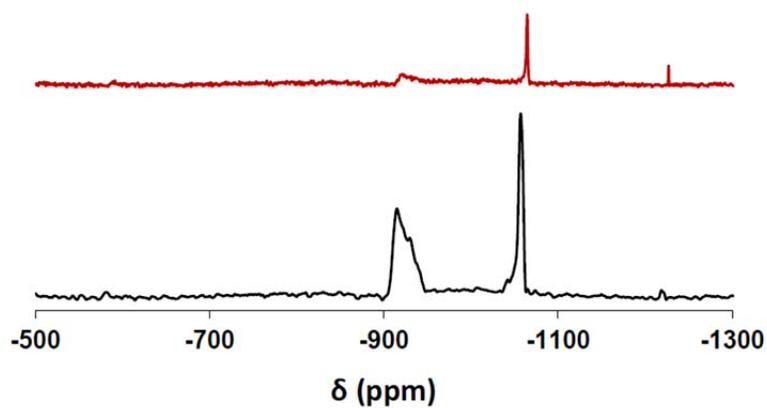
Figure 9.   Solution ^{99}Tc NMR Spectra of $[Tc(CO)_3 \cdot EDTA]^{n-}$ (δ = -918 ppm) in 5 M $NaNO_3$/0.1 M NaOH (bottom, black trace) and in Simulant (top, red trace). The resonance at δ = -1070 ppm is due to $[Tc(CO)_3(H_2O)_2(OH)]$ species.
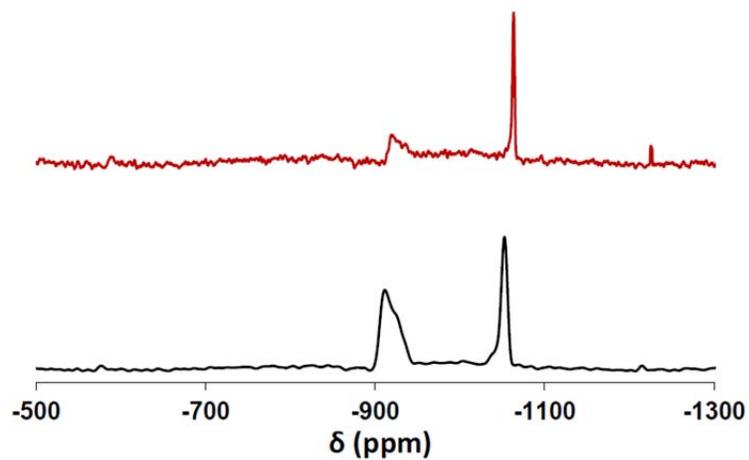
Figure 10. Solution ^{99}Tc NMR Spectra of $[Tc(CO)_3 \cdot NTA]^{n-}$ (δ = -916 ppm) in 5 M $NaNO_3$/0.1 M NaOH (bottom, black trace) and in Simulant (top, red trace). The resonance at δ = -1070 ppm is due to $[Tc(CO)_3(H_2O)_2(OH)]$ species.
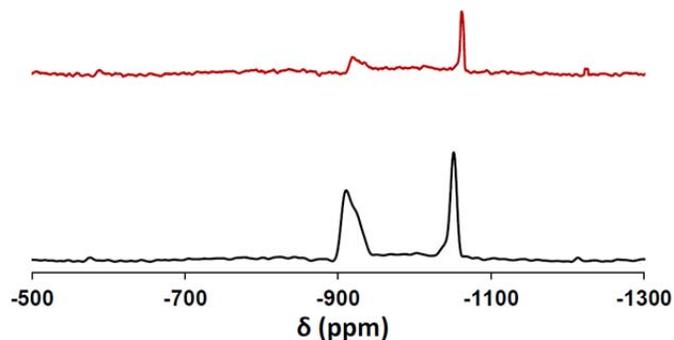
Figure 11. Solution ^{99}Tc NMR Spectra of [Tc(CO)$_3$•DTPA]$^{n-}$ (δ = -915 ppm) in 5 M NaNO$_3$/0.1 M NaOH (bottom, black trace) and in Simulant (top, red trace). The resonance at δ = -1070 ppm is due to [Tc(CO)$_3$(H$_2$O)$_2$(OH)] species.

Gluconate effectively coordinates to [Tc(CO)$_3$]$^+$, resulting in nearly quantitative conversion of [Tc(CO)$_3$(H$_2$O)$_2$(OH)] to [Tc(CO)$_3$•Gluconate]$^{n-}$ (Figure 12). In 5 M NaNO$_3$/0.1 M NaOH solution, the complexation process is completed in about 4 – 8 hours, and 85% of Tc(I) is converted to [Tc(CO)$_3$•Gluconate]$^{n-}$ form as characterized by the appearance of the resonances at -1100, -1232, and -1354 ppm, indicating three inequivalent Tc(I) environments generated upon gluconate coordination; the structure of the [Tc(CO)$_3$•Gluconate]$^{n-}$ species is currently being elucidated. The remaining Tc is oxidized to TcO$_4^-$. In the simulant, however, a lower fraction (~70%) of Tc(I) is converted to the [Tc(CO)$_3$•Gluconate]$^{n-}$ complex, with ~15% remaining as [Tc(CO)$_3$(H$_2$O)$_2$(OH)] and the rest oxidized to TcO$_4^-$.
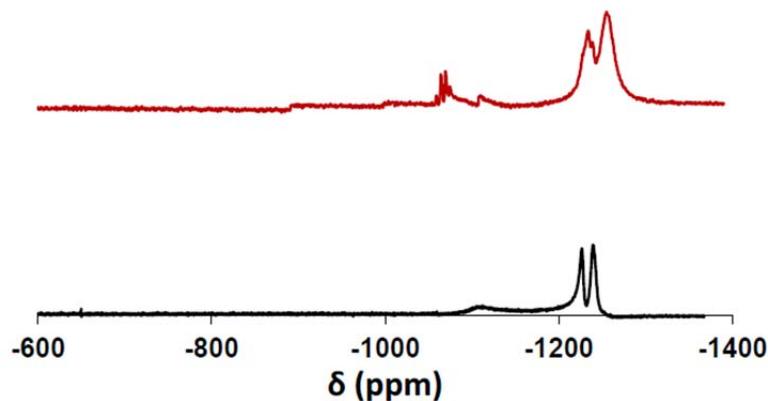
Figure 12. Solution ^{99}Tc NMR Spectra of [Tc(CO)$_3$•Gluconate]$^{n-}$ (δ = -1100, -1232, and -1354 ppm) in 5 M NaNO$_3$/0.1 M NaOH (bottom, black trace) and in Simulant (top, red trace). The resonance at δ = -1070 ppm is due to [Tc(CO)$_3$(H$_2$O)$_2$(OH)] species.

The IDA ligand exhibits a remarkably high affinity towards $[Tc(CO)_3]^+$ in both 5 M $NaNO_3$/0.1 M NaOH and simulant. The NMR spectra of the $[Tc(CO)_3\cdot IDA]^{n-}$ product in both the matrices are characterized by an intense resonance at -998 ppm, with a weaker, broader resonance at -850 (Figure 13). It is also worth noting that the kinetics of $[Tc(CO)_3(IDA)]^{n-}$ formation is fast, resulting in complete conversion of $[Tc(CO)_3(H_2O)_2(OH)]$ to $[Tc(CO)_3\cdot IDA]^{n-}$ within 30 minutes.
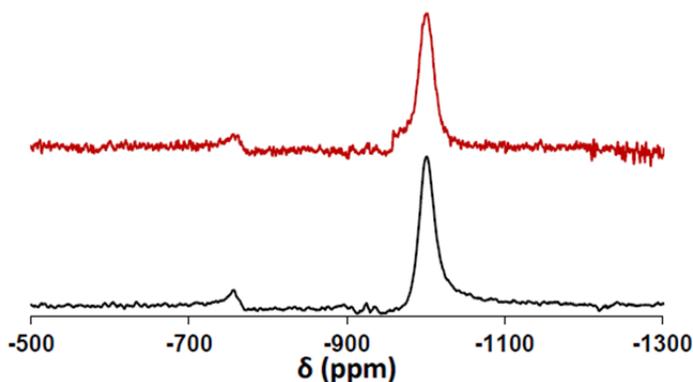
Figure 13. Solution ^{99}Tc NMR Spectra of $[Tc(CO)_3\cdot IDA]^{n-}$ (δ = -850 and -998 ppm) in 5 M
$NaNO_3$/0.1 M NaOH (bottom, black trace) and in Simulant (top, red trace)

4.2   Infrared (IR) Spectroscopy

In characterizing the $[Tc(CO)_3]^+$ compounds, IR spectroscopy is most useful for identification of Tc-CO bonds which generate distinct fingerprint signals occurring in a spectral region where little potential interferences exist. So with appropriate detector and sufficient number of scans we can observe high micro molar concentrations of Tc(I) carbonyl compounds. It can potentially provide useful structural information to compliment NMR technique. There is no precedent of IR measurements of the actual tank waste, however it remains to be attractive techniques due to its simplicity and availability (Serne et al. 2014).

4.2.1   FTIR Spectroscopy of the Starting Materials

4.2.1.1   (Et_4N)_2[Tc(CO)_3Cl_3]

The IR spectrum of the isolated solid $(Et_4N)_2[Tc(CO)_3Cl_3]$ material showed the presence of the characteristic Tc-CO vibration bands at 1980, 1871, and 1844 cm^{-1} (Figure 14). The band at 1871 cm^{-1} appears as a shoulder to the intense band at 1844 cm^{-1}. These bands are attributed to the symmetric in-plane, symmetric out-of-plane, and asymmetric stretches (Alberto et al. 1995; Dattelbaum et al. 2002). Computational models developed in this study revealed that these vibrations result from the contributions from all three CO groups. Weak bands appearing at 2989 cm^{-1} and 2956 cm^{-1} are assigned to C-H stretches (Alberto et al. 1995). The bands in the crowded fingerprint region are also in agreement with the ones reported for the $(Et_4N)_2[Tc(CO)_3Cl_3]$ compound (Alberto et al. 1995) shown in parentheses: 1462 (1458), 1181 (1184), 795 (798), 675 (668), 648 (638), and 485 (500) cm^{-1}. Several additional bands are

observed at 1402, 1398, 1307, 1003, 921, and 900 cm^{-1}. Overall consistently with NMR measurements, IR spectral features confirm the structure and high purity of the $(Et_4N)_2[Tc(CO)_3Cl_3]$ material.
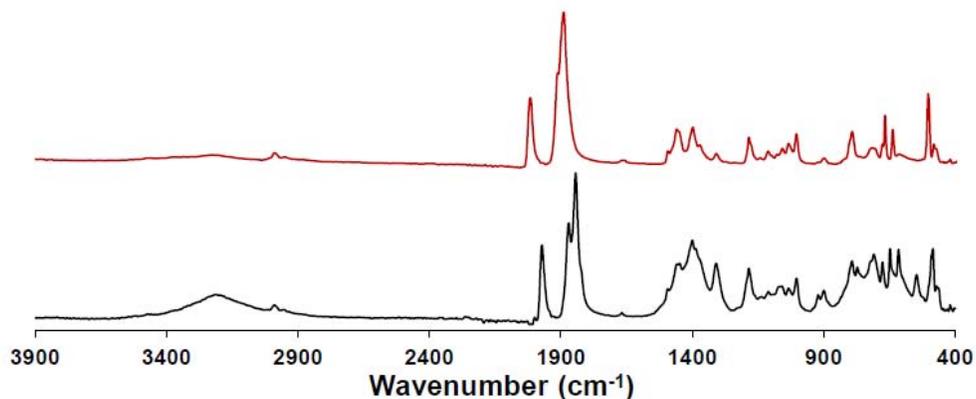
Figure 14. Infrared Spectra of the Solid (bottom, black trace) and MeCN Solution (top, red trace) of $(Et_4N)_2[Tc(CO)_3Cl_3]$

The IR spectrum of the MeCN solution of $(Et_4N)_2[Tc(CO)_3Cl_3]$ demonstrated that the characteristic CO vibrations are shifted to the higher energy in comparison with the solid material and appear at 2017, 1913 (shoulder), and 1889 cm^{-1} (Figure 14 and Figure 15). The bands in the fingerprint region showed at 1454, 1398, 1184, 1004, 791, 667, 636, and 500 cm^{-1}. The differences between solid and MeCN solution of $(Et_4N)_2[Tc(CO)_3Cl_3]$ are attributed to the exchange of chloride with MeCN in solution as observed by the NMR measurements.
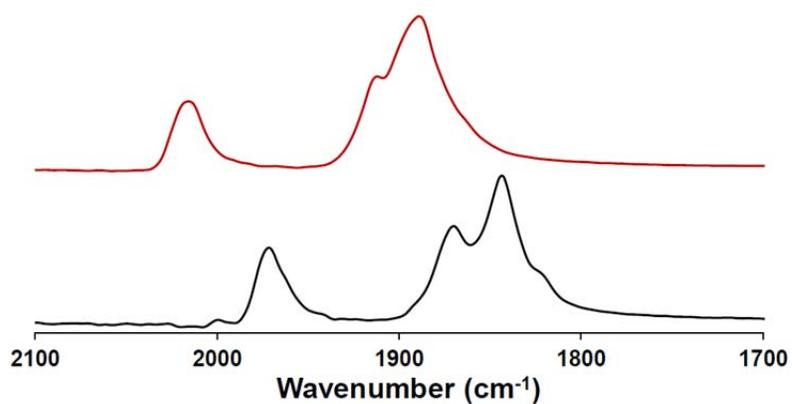
Figure 15. Carbonyl IR Spectral Region of the Solid (bottom, black trace) and MeCN Solution (top, red trace) of $(Et_4N)_2[Tc(CO)_3Cl_3]$

4.2.1.2   [Tc(CO)$_3$(OH)]$_4$

The IR spectrum of the solid [Tc(CO)$_3$(OH)]$_4$ tetramer demonstrated a sharp band at 2032 cm^{-1} and a broad band at 1925 cm^{-1} in the CO region (Figure 16). The broad band is assumed to be the overlap of the symmetric and asymmetric C-O stretches. These bands are in agreement with those previously observed for [Tc(CO)$_3$(OH)]$_4$ at 2044 and 1919 cm^{-1} (Alberto et al. 1998). The bands observed at 844 and 797 cm^{-1} are also in agreement with the same report (835 and 792 cm^{-1}). Fingerprint bands appeared at 1382, 1352, 1117, 1076, and 1043 cm^{-1}.
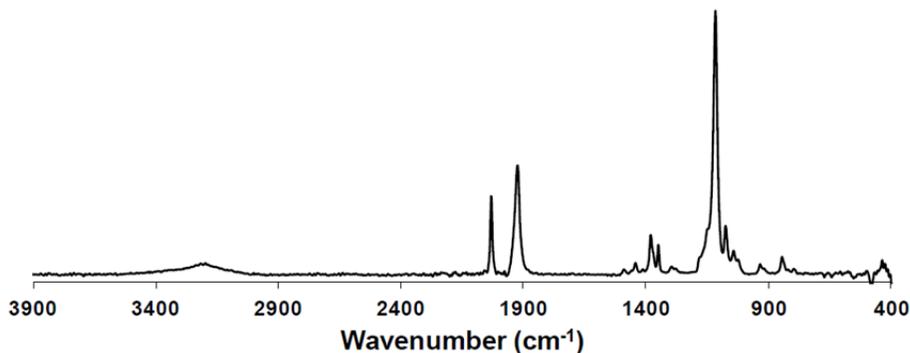
Figure 16. Infrared Spectrum of the Solid [Tc(CO)$_3$(OH)]$_4$ Tetramer

4.2.2   Solution FTIR Spectroscopy of [Tc(CO)$_3$(H$_2$O)$_{3-n}$(OH)$_n$]$^{1-n}$ and [Tc(CO)$_3$•Ligand]$^{n-}$ Complexes

The IR fingerprint region (<1300 cm^{-1}) of the aqueous 5 M NaNO$_3$/0.1 M NaOH and simulant solutions contains interfering bands due to the oxy-anions, and therefore is unsuitable for the identification of the solutes. However, the carbonyl spectral region (1700-2500 cm^{-1}) is devoid of spectral interferences and can be useful for the determination of the [Tc(CO)$_3$]$^+$ species. The solutions containing weak complexing agents such as NTA, EDTA, and DTPA as well as [Tc(CO)$_3$(H$_2$O)$_2$(OH)] species generated IR spectra nearly identical to that of a [Tc(CO)$_3$(H$_2$O)$_2$(OH)] solution (not shown). The IR spectral overlay of the [Tc(CO)$_3$(H$_2$O)$_{3-n}$(OH)$_n$]$^{1-n}$, and [Tc(CO)$_3$•Gluconate]$^{n-}$ and [Tc(CO)$_3$•IDA]$^{n-}$ compounds in the carbonyl region shown in Figure 17, demonstrates structure-dependent characteristic CO vibrations. The CO vibrations are listed in Table 3. Gluconate and IDA complexes show multiple vibrations in the Tc-carbonyl region (1700-2500 cm^{-1}) which are attributed to carboxylate vibrations of the Tc-coordinated ligands in addition to the characteristic Tc-CO vibrations arising from the [Tc(CO)$_3$]$^+$ backbone.
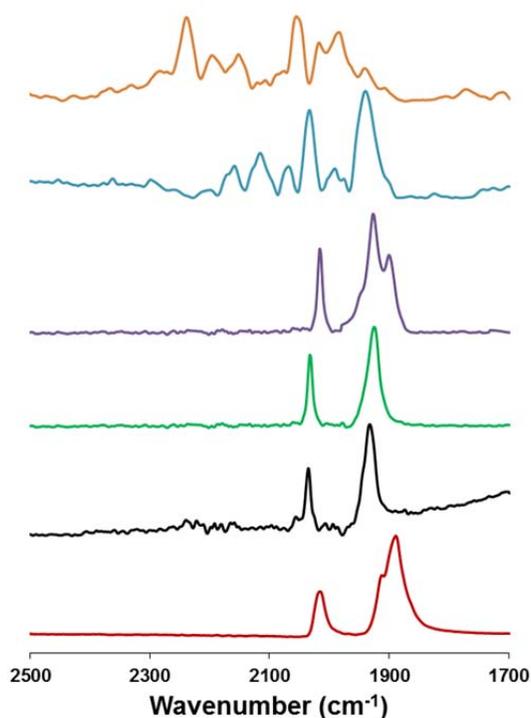
Figure 17. Carbonyl IR Spectral Region of the $[Tc(CO)_3]^+$ Species in Solution. Bottom, red trace: $[Tc(CO)_3Cl_3]^{2-}$ in MeCN. Second from bottom, black trace: $[Tc(CO)_3(H_2O)_3]^+$ in 5 M NaNO_3 at pH = 0 – 6. Third from bottom, green trace: $[Tc(CO)_3(OH)]_4$ in 5 M NaNO_3 at pH = 7 – 11. Third from top, violet trace: $[Tc(CO)_3(H_2O)_2(OH)]$ in 5 M NaNO_3/0.1 M NaOH. Second from top, blue trace: $[Tc(CO)_3 \cdot Gluconate]^{n-}$ in 5 M NaNO_3/0.1 M NaOH. Top, orange trace: $[Tc(CO)_3 \cdot IDA]^{n-}$ in 5 M NaNO_3/0.1 M NaOH.

Table 3. Tabulation of the IR Vibrations of the $[Tc(CO)_3]^+$ Compounds in the Tc-CO Region

Complex	CO Vibrations (cm^{-1})
$[Tc(CO)_3(H_2O)_3]^+$	1931, 1943(sh), 2036
$[Tc(CO)_3(OH)]_4$	1925, 1939(sh), 2032
$[Tc(CO)_3(H_2O)_2(OH)]$	1898, 1923, 1945(sh), 2016
$[Tc(CO)_3 \cdot Gluconate]^{n-}$	2162, 2115, 2067, 1989, 1937, 1956(sh), 2034
$[Tc(CO)_3 \cdot IDA]^{n-}$	2243, 2193, 2152, 2051, 2012, 1981, 1939

4.3   Tc Electron Paramagnetic Resonance (EPR) Spectroscopy

Similar to NMR spectroscopy, EPR spectroscopy measures the transition of an unpaired spin in an external magnetic field from a low energy state in line with the external magnetic field to a high energy state antiparallel to the external magnetic field. However, rather than directly probing unpaired nuclear spin as is the case with NMR, EPR directly probes unpaired electron spin. EPR measurements can be performed in solid or solution state and generated signals are responsive to the chemical environment of atoms over which the unpaired electron spin is delocalized. Technetium in oxidation states of II, IV, and

VI has an outer electron configuration of $4d^5$, $4d^3$, and $4d^1$, respectively, and is therefore paramagnetic and susceptible to measurements by EPR spectroscopy. Technetium EPR spectroscopy is most suited for these paramagnetic oxidation states of Tc that cannot be observed by ^{99}Tc NMR; in this sense, EPR and NMR complement each other, allowing observation of Tc in most oxidation states. To date, EPR has not been applied to analysis of Hanford tank supernatants, and developmental work is needed to address questions about potential interferences and to identify the detectable concentrations of various Tc species. If developed, the EPR method can provide useful information for identification of non-pertechnetate species in the tank waste, including oxidation state and chemical environment of Tc compounds in the even oxidation states.

In 2014, development of the Tc EPR method was initiated using a standard Tc(V) compound, $[TcOCl_4]^-$, existing in equilibrium with the EPR-active Tc(VI) species, $[TcOCl_5]^{2-}$ (Levitskaia et al. 2014). Technetium in the oxidation state of IV was tested by EPR using $[Tc(IV)Cl_6]^{2-}$. It was observed that Tc(IV) and Tc(VI) generate strong and distinct spectra even at trace concentration levels. Based on these promising results, Tc EPR is applied in this work for identification of non-pertechnetate Tc(IV) and Tc(VI) species in oxidation states unsuitable for Tc NMR spectroscopy.

FY 2015 EPR experimentation included three activities summarized below.

Activity 1. Electrochemical generation and EPR measurements of Tc(IV) and Tc(VI) in 5 M $NaNO_3$/variable NaOH solutions. The electrochemical synthesis method provides the advantages of controlled reaction conditions and generation of material with known Tc oxidation state and chemical environment. These samples were used to properly tune the EPR instrument and develop methods for the Tc measurements in complex matrices. These samples can provide reliable EPR spectral information suitable for identification of the Tc(IV) and Tc(VI) species in complex mixtures.

Activity 2. EPR measurements of the Tc(IV) and Tc(VI) samples chemically generated by reduction of TcO_4^- by CO/H_2 reductant in the simulant with and without gluconate and catalytic noble metals as described in our FY 2014 report (Levitskaia et al. 2014). In these studies, the EPR method developed under Activity 1 is utilized, and EPR spectra of Tc(IV) and Tc(VI) generated in simple 5 M $NaNO_3$ solutions served as controls for comparison purposes. The EPR measurements of the chemically generated Tc(IV) species are currently in progress and will be discussed in follow-up reports.

Activity 3. EPR measurements of the Tc(I) $(Et_4N)_2[Tc(CO)_3Cl_3]$ and $[Tc(CO)_3(OH)]_4$ compounds to check for the presence of Tc impurities in +2, +4, and +6 oxidation states using the EPR method developed under Activity 1. It was observed that the acquired EPR spectra contained no signals due to Tc species, confirming Tc(I) oxidation state purity in agreement with the NMR results described in Section 4.1. of this report. No further description of these measurements is included in this report.

4.3.1   Spectroelectrochemical Generation and Monitoring of Tc (IV) and Tc (VI)

To evaluate the spectroelectrochemical behavior of $TcO4^-$ in 5 M $NaNO_3$ solutions, absorption-based double potential step chronoabsorptometry was employed. The initial potential was set to -0.1 V to ensure that all of the Tc in the sample is present in the fully oxidized TcO_4^- state, while absorption spectra were concurrently recorded. Subsequently, the working potential was set to a given value (E_{app}), and the solution was allowed to reach equilibrium, which was inferred when the UV-visible absorption spectrum no longer changed over a 3–4 min period. Shown in Figure 18 are the absorption spectra at each potential

as E_{app} was decreased in a stepwise fashion. This allowed for measurements on the fully oxidized TcO4⁻ and fully reduced forms, as well as intermediate mixtures. Reversing the step direction or varying the step size gave the same spectral results (not shown). Spectroelectrochemistry for the first process shows isosbestic behavior, suggesting presence of two equilibrium species. At the most negative potential, the quantitative conversion of TcO_4^- to TcO_4^{2-} product was observed. The spectroelectrochemical titration data thus obtained were analyzed according to the Nernstian equation for electron transfer reaction, which shows a 1 e⁻ transfer. This is suggestive of a one-electron process as described by reaction (2).

$$TcO_4^- + e^- = TcO_4^{2-} \qquad (2)$$

Beyond -800 mV, there is deposition of black precipitate on the working electrode surface, which further reduces the absorbance by obstructing the light path. This precipitate is presumably insoluble TcO_2 formed by the reduction of TcO_4^{2-} that deposits on the electrode surface.
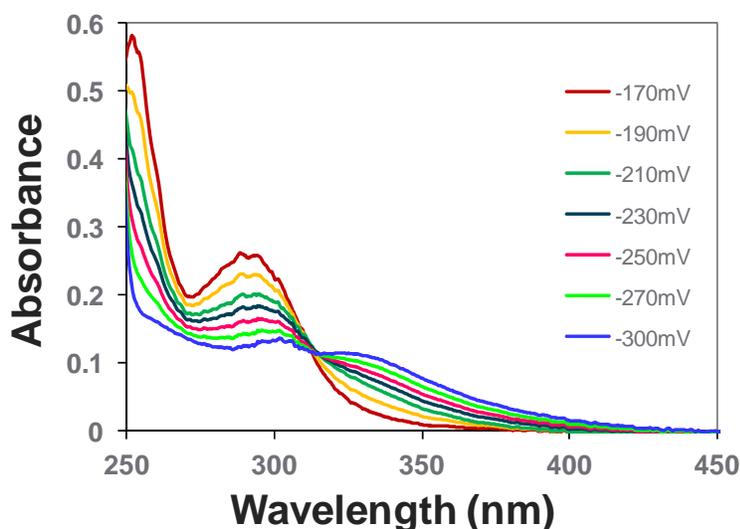
Figure 18. UV-vis Monitoring of Electrochemical Reduction of TcO_4^- to TcO_4^{2-}, Demonstrating Isosbestic Behavior

4.3.2   EPR Spectroscopy of Electrochemically Generated Tc (VI) Species

EPR spectra are analyzed primarily through examination of two experimental parameters known as the g-value, and the a-value. The g-value is a dimensionless measure of the strength of the magnetic field generated by the unpaired electron, which is being experimentally probed. Small changes in the chemical environment correspond to a shift in observed g-value relative to that of an unbound electron. This is analogous to chemical shift measured in NMR spectroscopy, and can be used as evidence of metal oxidation state and chemical composition.

When an electron with unpaired spin is in the presence of nuclei which also have unpaired spin, interaction takes place that results in the single spectral response of the unpaired electron being split into multiple resonances. This splitting of the signal is known as hyperfine splitting, and the a-value is a measurement of the magnitude of splitting, which in turn is determined by the strength of the interaction between the electron and nucleus as well as the nuclear magnetic moment. The number of resonances

lines that the signal is split into is determined by 2nI+1 where n is the number of nuclei the electron is interacting with and I is the nuclear spin of those nuclei. Thus, EPR is an effective tool to measure chemical and isotopic composition provided unpaired electron spin is present.

Samples of TcO_4^- in a 5 M $NaNO_3$/2 M NaOH solution were subjected to a working electrode potential of -800 mV vs. a Ag/AgCl reference electrode in order to generate a sample of Tc(VI). The solution in the vicinity of the working electrode surface was collected and subjected to EPR spectroscopy experiments at 125 K. The representative results for the 5 M $NaNO_3$/2 M NaOH solution are described below.

The Tc(VI) EPR spectrum in 5 M $NaNO_3$/2 M NaOH is show in Figure 19. Examination of the spectrum shows evidence of an axial spin system (two of three axes in the atomic reference frame are degenerate) with an overlap of 10 resonances for g_l and 10 resonances for g perpendicular. The sharp spectral response in combination with observed hyperfine splitting and approximate g-value is consistent with an electron spin ½ system in which spin density primarily resides on a ^{99}Tc nucleus in near cubic symmetry. Due to the electrochemical potential at which the samples were generated (Rard 1983) coupled with UV-vis spectroelectrochemical determination of electron transfer stoichiometry through Nernstian analysis (see Section 4.3.1), we feel confident that this EPR spectrum is due to a Tc(VI) TcO_4^{2-} species.

Least-squares fitting of the spectrum was carried out with the Easyspin software package (Stoll and Schweiger 2006) in order to extract experimental g-values and a-values. Despite the apparent axial nature of the EPR spectrum, all axes in the molecular frame were allowed to vary independently during the least-squares fit. Values converged to an approximately $g_1 \sim g_2 < g_3$ and $a_1 \sim a_2 < a_3$ arrangement consistent with near degeneracy about two about two axes. The results are summarized in Table 4.
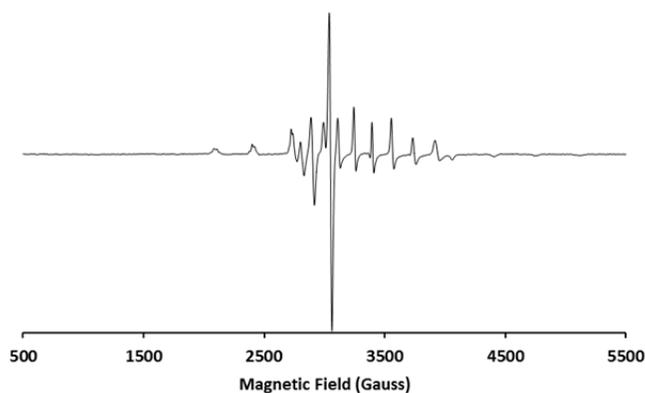
Figure 19. EPR Spectrum of Tc(VI) TcO_4^{2-} Species Generated Electrochemically from TcO_4^-

Table 4. Parameters Used to Perform Least-squares Fitting of Experimental EPR Spectra

Species	g_1	g_2	g_3	a_{Tc1} (MHz)	a_{Tc2} (MHz)	a_{Tc3} (MHz)	Line Width
Electrochemically generated Tc(VI)	2.033	2.019	1.894	367	359	-905	2.08
Chemically generated Tc(VI)	1.999	1.999	1.845	367	367	-900	4.28

4.3.3   EPR Spectroscopy of Chemically Generated Tc (VI) Species

As aforementioned, the EPR technique is being evaluated for use in determining Tc species in Hanford tank waste. Therefore, a product obtained from the chemical reduction of TcO_4^- in the simulant solution in presence of CO at elevated temperature and pressure as described in our previous report (Levitskaia et al. 2014) was subjected to analysis by EPR spectroscopy. The resulting spectrum can be seen in Figure 20. This spectrum shows many similarities to that of Figure 19, albeit considerable line broadening is present, which is attributable to the more complex chemical composition of the reaction mixture present. An overlay of these two spectra can be seen in Figure 21. The frequency shift between these two spectra is due to the different chemical environment of Tc(VI) as well as to a minor shift of microwave frequency of the EPR instrument (9.626635 vs. 9.625497 GHz). Hyperfine constants and g values from the simulation of electrochemically species were used as a starting point to simulate the spectrum seen in Figure 21, and a reasonable fit was obtained with only minor adjustment of the parameters. This suggests a Tc(VI) species of similar geometry is likely responsible for the spectrum in Figure 21. Due to the present of gluconate, which is highly coordinating, this species is attributed to Tc(VI)•gluconate complex. Like the spectrum in Figure 19, this spectral signature shows remarkable persistence, with the generated signal being observable up to a full year later (this is subject of the follow-up Task 3 report).

Additionally, close examination of downfield peaks of each spectrum shows a similar splitting pattern in each spectrum. Unfortunately the width of splitting is approximately the same as the line width, so determination of the nature of this splitting from the least-squares fitting is unreliable.

The chemically generated Tc(VI) species has been found to be remarkably stable, with a single solution store at room temperature being capable of generating a spectral response in excess of a year after generation.
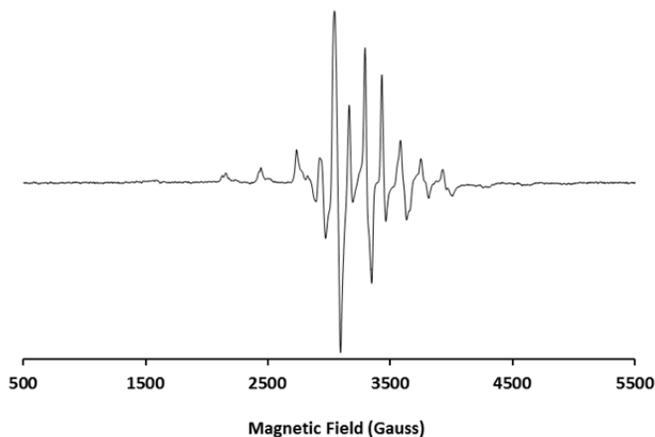
Figure 20. EPR Spectrum of Tc(VI) Species Generated Chemically from TcO_4^- in Presence of Gluconate
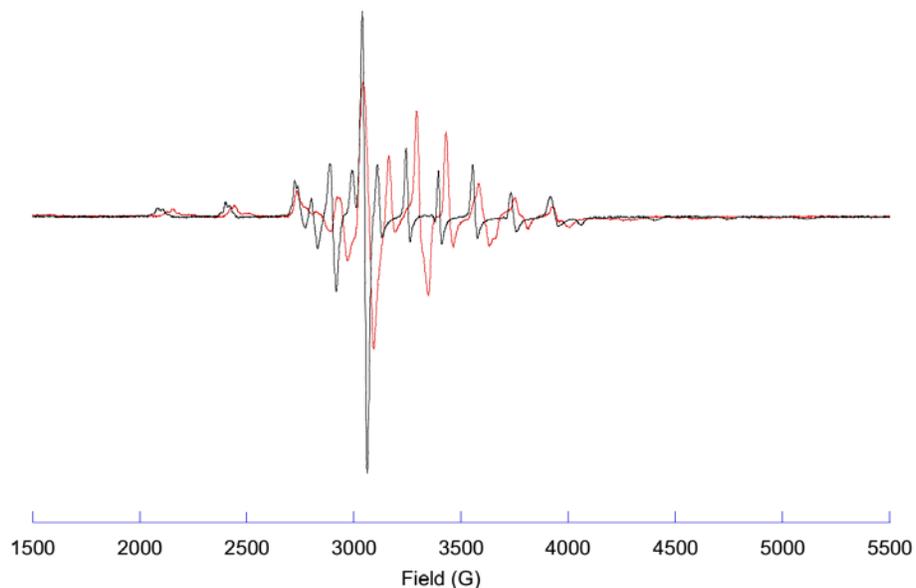
Figure 21. EPR Overlay of Electrochemically Generated Tc(VI) TcO_4^{2-} Species (black trace) and Chemically Synthesized Tc(VI) Species in Presence of Gluconate (red trace)

4.3.4   EPR Spectroscopy of Electrochemically Generated Tc(IV) Species

Tc(IV) species were generated electrochemically by holding the solution at -1,000 mV vs. a Ag/AgCl reference electrode, wherein the product was electrodeposited on the surface of the working electrode. The working electrode was then subjected to EPR spectroscopy experiments. Spectra due to Tc(IV) species are anticipated to have a more complex appearance and considerable line broadening over Tc(VI) species due to the increased total electron spin of the system to greater than ½. As can be seen in Figure 22, line broadening due to the quartet ground state has caused line broadening to such a degree that specific hyperfine interactions are difficult to discern.
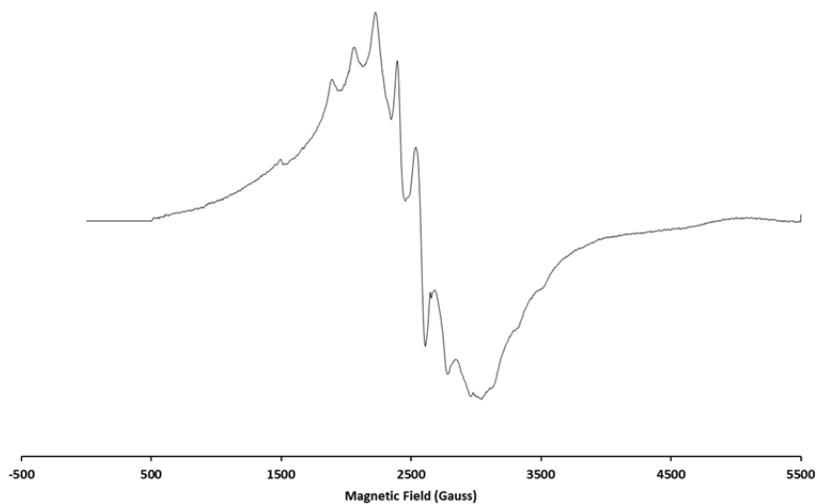
Figure 22. EPR Spectrum of Solid Tc(IV) Species Generated Electrochemically from TcO_4^-

5.0   Discussion

The emphasis of the FY 2015 work described in this report was on understanding spectroscopic signatures and development of the library of Tc(I) compounds derived from the $[Tc(CO)_3]^+$ core. The compiled database includes ^{99}Tc NMR, IR, and EPR characterization of the $[Tc(CO)_3(H_2O)_{3-n}(OH)_n]^{1-n}$ and $[Tc(CO)_3\bullet Gluconate]^{n-}$ compounds. The structures of the $[Tc(CO)_3]^+$ species included in the database are given in Figure 22.

The obtained ^{99}Tc NMR spectroscopic database is summarized in Table 5. The NMR data for all compounds are nearly identical in all the solution matrices, including water, 5 M NaNO$_3$, or simulant, demonstrating that anions (other than hydroxide) typifying tank supernatant matrix exhibit no interaction with the $[Tc(CO)_3]^+$ framework. This finding is important for utilization of NMR spectroscopy for the identification of the $[Tc(CO)_3]^+$ species in Hanford tank waste.

The compositions of the $[Tc(CO)_3(H_2O)_{3-n}(OH)_n]^{1-n}$ species depend on the solution alkalinity and can be easily identified by their distinct chemical shifts and half-line widths. The triaqua $[Tc(CO)_3(H_2O)_3]^+$ only exists in acidic solutions, and starts undergoing extensive deprotonation starting at near-neutral pHs. Therefore, $[Tc(CO)_3(H_2O)_3]^+$ is unlikely to exist in the tank waste. The mono-hydroxo species $[Tc(CO)_3(H_2O)_2(OH)]$ is observed to be persistent in alkaline solutions, though at high Tc concentrations it can undergo oligomerization to form the tetrameric species $[Tc(CO)_3(OH)]_4$ over time, which is stable in the intermediate pH range (pH= 6.5 to 11). At high concentrations of OH$^-$, the $[Tc(CO)_3(H_2O)(OH)_2]^-$ species is also observed, though $[Tc(CO)_3(H_2O)_2(OH)]$ is the predominant species. At very high hydroxide concentrations, it is possible to see the $[Tc(CO)_3(OH)_3]^{2-}$ species.
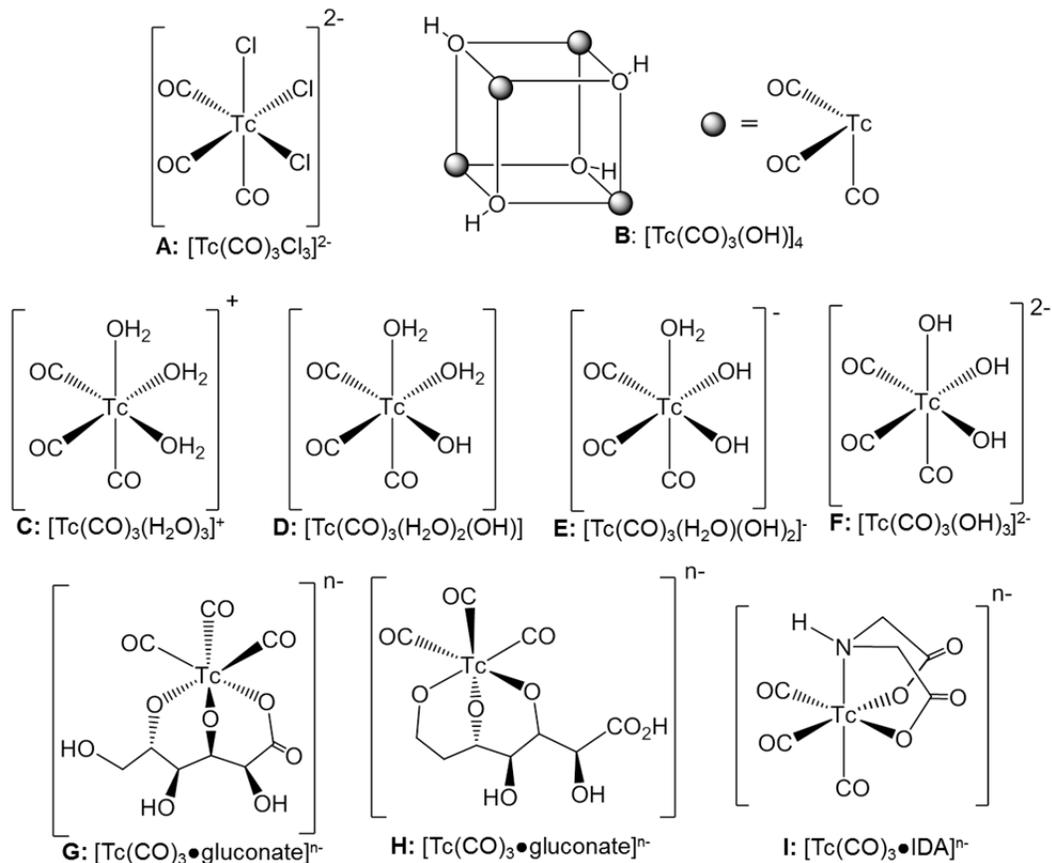
Figure 23. Molecular Structures of the Starting $[Tc(CO)_3Cl_3]^{2-}$ Material and $[Tc(CO)_3]^+$ Complexes Included in the Spectral Database

Density functional theory computations are being used to model the $[Tc(CO)_3(H_2O)_{3-n}(OH)_n]^{1-n}$ spectra that are being experimentally generated during construction of the spectral library. Despite the difficulties in modeling a highly challenging solvent system with strong intermolecular interactions such as hydrogen-bonding, the DFT computations are able to closely estimate chemical shifts present in ^{99}Tc NMR spectra, as can be seen in Table 5. For the systems with well-defined chemical structures in aqueous solvent similar to tank waste conditions, DFT computations are predicting chemical shifts to within 100 ppm in a Tc spectral window that is greater than 10,000 ppm wide. Many of the species modeled, particularly the tricarbonyl aqua and tricarbonyl hydroxide species, are modeled even more accurately and fall within 40 ppm of the experimentally observed signals. Given the large range present in the ^{99}Tc NMR spectral window, DFT computations have proved a valuable tool for structural verification and identification of ^{99}Tc NMR assignments for new species.

Table 5. ^{99}Tc NMR Spectroscopic Database of the $[Tc(CO)_3]^+$ Compounds

Complex	Solvent	Experimental ^{99}Tc NMR Chemical Shift (ppm)	Half Width of ^{99}Tc Resonance (Hz)	Calculated ^{99}Tc NMR Chemical Shift (ppm)	Absolute Deviation from Experiment (ppm)
TcO_4^-	H$_2$O	-3 – +3	20	0	0
	5 M NaNO$_3$/NaOH	-3 – +3	20	0	0
	Simulant	-3 – +3	20	0	0
$[Tc(CO)_3(H_2O)_3]^+$	5 M NaNO$_3$/HNO$_3$ pH = 0 – 7	-868	100	-837	31
$Tc(CO)_3(OH)]_4$	H$_2$O	-583	480	-620	37
	5 M NaNO$_3$/NaOH pH = 7 – 11	-585	480	-620	35
	Simulant	-590	500	-	-
$[Tc(CO)_3(H_2O)_2(OH)]$	5 M NaNO$_3$/0.01 – 10 M NaOH	-1062	90	-1067	5
	Simulant	-1070	100	-	-
$[Tc(CO)_3(H_2O)(OH)_2]^-$	5 M NaNO$_3$/3 – 10 M NaOH	-1140	110	-1173	33
$[Tc(CO)_3(OH)_3]^{2-}$	5vM NaNO$_3$/>10 M NaOH	-1210	130	-1305	95
$[Tc(CO)_3\bullet(DTPA)]^-$	5 M NaNO$_3$/0.1 M NaOH	-915	600	Not calculated	N/A
	Simulant	-910	700		
$[Tc(CO)_3\bullet(NTA)]^-$	5 M NaNO$_3$/0.1 M NaOH	-918	550		
	Simulant	-915	650		
$[Tc(CO)_3\bullet(EDTA)]^-$	5 M NaNO$_3$/0.1 M NaOH	-916	550		
	Simulant	-920	650		
$[Tc(CO)_3\bullet(IDA)]^-$	5 M NaNO$_3$/0.1 M NaOH	-850 (broad) -998	1000 700	Calculations are currently underway	N/A
	Simulant	-820 -1000	1000 750		
$[Tc(CO)_3\bullet(gluconate)]^{n-}$	5 M NaNO$_3$/0.1 M NaOH	-1100 (broad) -1232 -1254	1000 650 550		
	Simulant	-1100 (broad) -1240 -1259	1000 700 600		

Among small chelators evaluated for the feasibility of the complex formation with $[Tc(CO)_3]^+$, only gluconate and IDA were found to form strong complexes, with IDA being the most coordinating, potentially due to coordination of the amino nitrogen in addition to carboxylic oxygen to the Tc center. NTA, EDTA, and DTPA formed weak complexes and were not able to effectively compete with hydroxide ligands for Tc coordination sites; therefore, their existence in the tank wastes is deemed unlikely.

While previous work (Lukens et al. 2004) had demonstrated the presence of $[Tc(CO)_3 \bullet Gluconate]^{n-}$ complex in Hanford tank waste from EXAFS analysis, the exact coordination environment around the Tc center had not been determined yet. Comprehensive analyses using ^{99}Tc NMR conducted in this work revealed that complexation of gluconate results in three distinct $[Tc(CO)_3 \bullet Gluconate]^{n-}$ chemical environments. Based on molecular modelling calculations, the resonances at -1232 and -1254 ppm are tentatively attributed to species **G** and **H** in Figure 23. The broad resonance at -1100 ppm is speculatively attributed to the polynuclear $[Tc(CO)_3 \bullet Gluconate]^{n-}$ species. Similarly, IDA also exhibits a remarkably high affinity towards $[Tc(CO)_3]^+$ in both 5 M $NaNO_3$/0.1 M NaOH and simulant, showing an intense resonance at about -1000 ppm and a weaker and broader resonance at about -850 ppm. The resonance at -1000 ppm is assigned to a $[Tc(CO)_3 \bullet IDA]^{n-}$ species whose structure is tentatively assigned to the structure **I** (Figure 23) based on a similar structure proposed by Rattat and coworkers during the reaction of $[^{99m}Tc(CO)_3(H_2O)_3]^+$ with IDA (Rattat et al. 2004).

Overall based on the assembled ^{99}Tc NMR spectral database, it is concluded that pertechnetate and the various $[Tc(CO)_3(H_2O)_{3-n}(OH)_n]^{1-n}$ and $[Tc(CO)_3 \bullet Ligand]^{n-}$ complexes, which presence can be anticipated in the tank waste, can be unambiguously identified by NMR spectroscopy provided they exist at concentration levels observable by this technique (high micromolar and above).

The obtained ^{99}Tc NMR spectroscopic database is summarized in Table 5. The IR-spectroscopic data demonstrate that the Tc-carbonyl region (1700-2500 cm^{-1}) is anticipated to be free from most interferences coming from various oxy-anions present in tank waste supernatants, and can be potentially utilized for the determination of the $[Tc(CO)_3(H_2O)_{3-n}(OH)_n]^{1-n}$ complexes. Identification of the $[Tc(CO)_3 \bullet Ligand]^{n-}$ compounds can be difficult due to the overlapping signals from the carboxylic group coordinated to Tc.

While Tc (VI) has traditionally been considered to be very short-lived, EPR signals observed from samples generated electrochemically and chemically have persisted, respectively, for in excess of one week and one year periods of time. This is an unexpected result from the current study and gives us a chance to interrogate an important intermediate in the redox steps between Tc (I) and Tc (VII). The spectrum of the electrochemically generated sample of TcO_4^{2-} shows many similarities to the spectrum resulting from the chemical reduction of TcO_4^- by CO/H_2, suggesting that similar species are responsible for both spectra. This is gives important insight to the mechanistic pathway of Tc(VII) reduction inside the tanks, as CO and H_2 are both present as auto-radiolysis products within the tanks.

Table 6. FTIR Spectroscopic Database of the $[Tc(CO)_3]^+$ Compounds

Complex	CO Vibrations (cm^{-1})	*DFT Calculated CO Vibrations (cm^{-1})
$[Tc(CO)_3Cl_3]^{2-}$	1889, 1915(sh), 2017	1885, 1885, 2052
$[Tc(CO)_3(H_2O)_3]^+$	1931, 1943(sh), 2036	1943, 1943, 2103
$[Tc(CO)_3(OH)]_4$	1925, 1939(sh), 2032	Calculations in progress
$[Tc(CO)_3(H_2O)_2(OH)]$	1898, 1923, 1945(sh), 2016	1899, 1901, 2056
$[Tc(CO)_3(Gluconate)]^{n-}$	2162, 2115, 2067, 1989, 1937, 1956(sh), 2034	Not calculated
$[Tc(CO)_3(IDA)]^-$	2243, 2193, 2152, 2051, 2012, 1981, 1939	Not calculated

DFT modelling has also been performed in order to predict the experimentally observed carbonyl stretching frequencies observed in FTIR spectroscopy. The tabulated results can be viewed in Table 6. Identical computational methods were used for the IR frequencies as were used in the ^{99}Tc NMR computations. The resulting in carbonyl stretching frequencies require a uniform shift of only 0.8% to be realigned with experimentally observed spectra. Given that inorganic carbonyl ligands are one of the few vibrations to occur in this region, coupled with drastic changes observed in inorganic carbonyl IR spectral signatures with minor changes in metal center electron density, and geometrical changes make this a powerful predictive tool.

6.0   Conclusions

In summary, ***this project developed stable forms of non-pertechnetate Tc including $[Tc(CO)_3•Ligand]^{n-}$ (where Ligand = IDA or Gluconate) and Tc(VI).*** The stability testing of these non-pertechnetates compounds is discussed in a separate report.

Various $[Tc(CO)_3]^+$ species that are potentially to be contained in Hanford tank waste have been synthesized and characterized by IR spectroscopy, ^{99}Tc NMR spectroscopy, and EPR spectroscopy. In conjunction with the aforementioned techniques, DFT computations are being benchmarked against the empirical results. This allows us to simultaneously pursue two routes towards determination of tank waste composition: characterizing the spectral fingerprints of individual species likely present in tank waste for facile identification of tank waste composition, and developing the capability to computationally predict the chemical structure of spectral signatures not yet catalogued in our database.

Each individual spectroscopic technique being utilized has its own distinct advantages and will provide fingerprint-like information about the individual components of tank waste. IR spectroscopy is suitable for analysis of the electronic and geometric structure of Tc compounds containing the $[Tc(CO)_3]^+$ moiety. The spectral region these moieties are observed in is populated by few other IR-active species, and the technique is sensitive to minute changes in molecular symmetry and metal center electron density, which in turn is related to Tc oxidation state. ^{99}Tc NMR spectroscopy is ideally suited for monitoring diamagnetic species with an even Tc oxidation state. Small changes in ligand substitution result in large changes in chemical shift, giving each compound a signature that is readily monitored. EPR spectroscopy is a complimentary technique to ^{99}Tc NMR and provides structural information on paramagnetic Tc

species, which are generally of an odd-numbered oxidation state and inaccessible via NMR spectroscopy. EPR spectroscopic measurements have very little interference from diamagnetic impurities present in solution, and thus EPR is an ideal technique for studying paramagnetic species in complex mixtures. This work demonstrates that Tc(VI) even at low concentrations generates a unique EPR signal suitable for identification of Tc this oxidation state. The observation that the Tc(VI) signal persists in the solution simulating tank waste supernatants encourages application of EPR techniques for the analysis of the actual tank wastes.

Based on the results of these measurements, ***it is proposed to use NMR, EPR, and IR spectroscopic techniques for Tc speciation analysis in the actual tank waste samples***.

DFT calculations complement each of these techniques individually, and this work expanded our understanding of computational parameters. The computations have been validated against our experimental ^{99}Tc NMR and IR spectra, and work is currently underway to benchmark the calculations against our experimental EPR spectroscopic measurements. Once fully benchmarked, the DFT computations will be used to predict species that are likely present in Hanford tank waste but difficult to synthetically access in a laboratory environment.

Work our team is currently pursuing will expand a comprehensive spectral database for Tc species potentially present in the Hanford tank waste in two directions. The first objective is aimed at the expansion of the available library of non-pertechnetate compounds in different oxidation states and chemical forms. Synthesis and spectroscopic characterization of Tc(I, II) carbonyl nitrosyl and Tc(IV, VI) species is in progress. In a companion effort, we are planning to expand the range of characterization techniques. X-ray absorption spectroscopy (XAS) can provide concrete evidence on Tc oxidation state as well as the identity of the first coordination sphere. X-ray adsorption near edge structure (XANES) and Extended X-ray absorption fine structure (EXAFS) spectroscopy have been previously utilized to gain information about the nature of n-Tc in actual Hanford tank waste supernatants (Blanchard et al. 1997; Lukens et al. 2004, 2006), but exact assignment of chemical species has been difficult due to a lack of EXAFS and XANES spectra on known Tc compounds.

The planned testing includes obtaining the actual waste samples collected from various Hanford tanks and their characterization for Tc speciation with NMR, EPR, IR, and XAS spectroscopies.

7.0   References

Aebischer N, R Schibli, R Alberto, and AE Merbach. 2000. "Complete Carbonylation of fac-[Tc(H2O)3(CO)3]+ under CO Pressure in Aqueous Media: A Single Sample Story!" *Agnew. Chem. Int. Ed.,*39, pp. 254-256.

Alberto R, R Schibli, A Egli, PA Schubiger, WA Herrmann, G Artus, U Abram, and TA Kaden. 1995. "Metal carbonyl syntheses XXII. Low pressure carbonylation of [MOCl$_4$]⁻ and [MO$_4$]⁻ the technetium(I) and rhenium(I) complexes [NEt$_4$]$_2$[MCl$_3$(CO)$_3$]." *J. Organomet. Chem.,* 493, pp. 119-127.

Alberto R, R Schibli, A Egli, U Abram, S Abram, TA Kaden, and PA Schubiger. 1998. "Steps towards [(C5Me5)TcO3]: Novel synthesis of [(C5Me5)Tc(CO)3] from [{Tc(p3-OH)(CO)3}4] and oxidation of [(C5Me5)M(CO)3] (M = Tc, Re) with Br2." *Polyhedron*, 17(7), pp. 1133 1140.

Blanchard Jr. DL, GN Brown, SD Conradson, SK Fadeff, GR Golcar, NJ Hess, GS Klinger, and DE Kurath. 1997. *Technetium in Alkaline, High-Salt, Radioactive Tank Waste Supernate: Preliminary Characterization and Removal*. PNNL-11386, Pacific Northwest National Laboratory, Richland, WA.

Cho H, WA de Jong, BK McNamara, BM Rapko, and IE Burgeson. 2004. Temperature and Isotope Substitution Effects on the Structure and NMR Properties of the Pertechnetate Ion in Water. *J. Am. Chem. Soc*. 126, 11583-11588.

Dattelbaum DM, KM Omberg, JR Schoonover, RL Martin, and TJ Meyer. 2002. "Application of Time-Resolved Infrared Spectroscopy to Electronic Structure in Metal-to-Ligand Charge-Transfer Excited States." *Inorg.Chem.,* 41, pp. 6071-6079.

Franklin KJ, CJL Lock, BG Sayer, and GJ Schrobilgen. 1982. "Chemical Applications of Technetium-99 NMR Spectroscopy: Preparation of Novel Technetium(VII) Species and Their Characterization by Multinuclear NMR Spectroscopy." *Journal of the American Chemical Society*, 104(20):5303-5306.

Golcar GR, NG Colton, JG Darab, and HD Smith. 2000*. Hanford Waste Tank Simulants Specification and Their Applicability for the Retrieval, Pretreatment, and Vitrification Processes*. PNWD-2455, Battelle--Pacific Northwest Division, Richland, WA.

Gorshkov NI, AA Lumpov, AE Miroslavov, and DN Suglobov. 2000. "Synthesis of $[Tc(CO)_3^+ \bullet (H_2O)_3]^+$ ion and investigation of its reaction with hydroxyl ion in the aqueous solutions." *Radiochemistry*, 45(2), pp: 116-119.

Levitskaia TG, A Anderson, SD Chatterjee, HM Cho, BM Rapko, JM Peterson, ED Walter, and NM Washton. 2014. "Speciation and Oxidative Stability of Alkaline Soluble, Non-Pertechnetate Technetium." PNNL-23654, EMSP-RPT-024, Rev. 0, Pacific Northwest National Laboratory, Richland, WA.

Lukens WW, DK Shuh, NC Schroeder, and KR Ashley. 2004. "Identification of the Non-Pertechnetate Species in Hanford Waste Tanks, Tc(I)-Carbonyl Complexes." *Environmental Science & Technology*, 38(1), pp. 229-33.

Lukens WW, DK Shu, NC Schroeder, and KR Ashley. 2006. *Behavior of Technetium in Alkaline Solution: Identification of the Non-Pertechnetate Species in High-Level Nuclear Waste Tanks at the Hanford Reservation*. Presented at ACS Symposium Series 943, Quincy, IL, 16 pp. American Chemical Society, Washington, DC.

Mikhalev VA. 2005. "^{99}Tc NMR Spectroscopy." *Radiochemistry* 47(4), pp. 319-33.

Neese F. 2012. "The ORCA program system." *Wiley Interdiscip. Rev.: Comput. Mol. Sci.*, 2, pp. 73–78.

Rapko BM, IE Burgeson, HM Cho, JR Deschane, AR Felmy, ED Jenson, BK McNamara, AP Poloski, LA Snow, and GT MacLean. 2003. *Mixing of WTP Process Solutions*. PNWD-3341, WTP-RPT-080, Rev. 0, Battelle–Pacific Northwest Division, Richland, WA.

Rapko BM, SA Bryan, S Chatterjee, MK Edwards, TG Levitskaia, JM Peterson, RA Peterson, and SI Sinkov. 2013. *Investigations into the Nature of Alkaline Soluble, Non-Pertechnetate Technetium*. PNNL-22957, EMSP-RPT-018, Pacific Northwest National Laboratory, Richland, WA.

Rard JA. 1983. "*Critical Review of the Chemistry and Thermodynamics of Technetium and Some of Its Inorganic Compounds and Aqueous Species*." Lawrence Livermore National Laboratory, UCRL-53440.

Rattat D, A Verbruggen, H Schmalle, H Berkeb, and R Alberto. 2004. "$[M(CO)_2(NO)]^{2+}$, a new core in bioorganometallic chemistry: model complexes of $[Re(CO)_2(NO)]^{2+}$ and $[^{99m}Tc(CO)_2(NO)]_2$." *Tetrahedron Lett.*, 45, pp. 4089–4092.

Schäfer A, H Horn, and R Ahlrichs. 1992. "Fully optimized contracted Gaussian basis sets for atoms Li to Kr." *J. Chem. Phys*. 97, pp. 2571-2577.

Scheele RD, GN Brown, and DE Kurath. 2009. *Scale-Up, Production, and Procurement of PEP Simulants*. PNNL-18678, WTP-RPT-204, Rev 0, Pacific Northwest National Laboratory, Richland WA.

Schroeder NC, SD Radzinski, KR Ashley, AP Truong, and PA Sczcepaniak. 1998. "Science and Technology for Disposal of Radioactive Tank Wastes." Schulz WW and NJ Lombardo, Eds.; Plenum Press: New York; pp. 301-320.

Schroll CA, S Chatterjee, WR Heineman, and SA Bryan. 2012. "Thin-Layer Spectroelectrochemistry on an Aqueous Microdrop." *Electroanalysis*, 24(5), pp. 1065 – 1070.

Serne RJ, BM Rapko, and IL Pegg. 2014. *Technetium Inventory, Distribution, and Speciation in Hanford Tanks*. PNNL-23319, Rev. 1; EMSP-RPT-022, Rev. 1, Pacific Northwest National Laboratory, Richland, WA.

Stoll S and A Schweiger. *"EasySpin, a comprehensive software package for spectral simulation and analysis in EPR."* 2006. *J. Magn. Reson.,* 178(1), pp. 42-55.

Weigend F and R Ahlrichs. 2005. "Balanced basis sets of split valence, triple zeta valence and quadruple zeta valence quality for H to Rn: Design and assessment of accuracy." *Phys. Chem. Chem. Phys.*, 7, pp. 3297-3305.

Distribution*

U.S. Department of Energy
Office of Environmental Management

NP Machara
SP Schneider

Pacific Northwest National Laboratory

A Andersen
SD Chatterjee
GB Hall
TG Levitskaia
RA Peterson
RJ Serne
ED Walter
NM Washton
Information Release   (PDF)

*All distribution will be made electronically.